Engineering Nanocomposite Materials for Cancer Therapy

*Caterina Minelli, Stuart B. Lowe, and Molly M. Stevens**

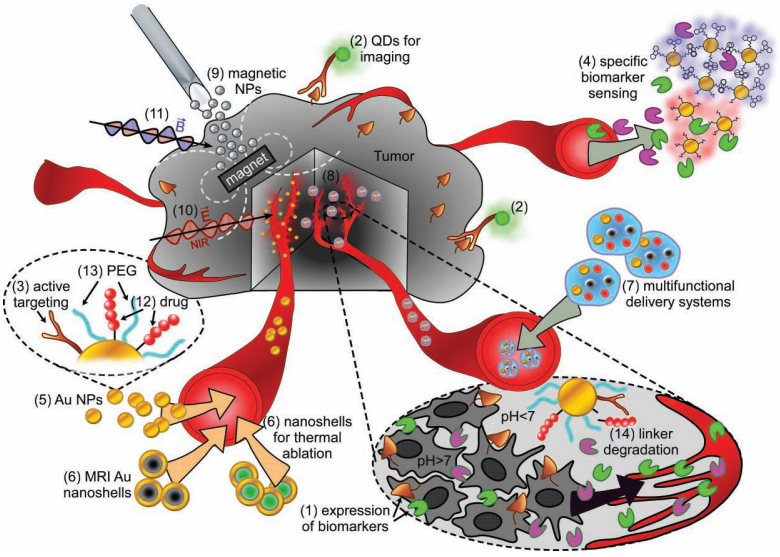

From the Contents

Cancer accounted for 13% of all deaths worldwide in 2005. Although early detection is critical for the successful treatment of many cancers, there are sensitivity limitations associated with current detection methodologies. Furthermore, many traditional anticancer drug treatments exhibit limited efficacy and cause high morbidity. The unique physical properties of nanoscale materials can be utilized to produce novel and effective sensors for cancer diagnosis, agents for tumor imaging, and therapeutics for cancer treatment. Functionalizing inorganic nanoparticles with biocompatible polymers and natural or rationally designed biomolecules offers a route towards engineering responsive and multifunctional composite systems. Although only a few such innovations have reached human clinical trial to date, nanocomposite materials based on functionalized metal and semiconductor nanoparticles promise to transform the way cancer is diagnosed and treated. This review summarizes the current state-of-the-art in the development of inorganic nanocomposites for cancer-related applications.

small NANO MICRO

1. Introduction

Directly or indirectly, cancer affects most people's lives, regardless of sex, social status, or age group. Alongside cardiovascular diseases, cancer is one of the leading causes of death and accounted for 7.4 million deaths worldwide in 2004.[1] In addition to causing pain and suffering, cancer can substantially affect a patient's ability to lead a normal life and often necessitates prolonged periods of hospitalization and informal care. These demands put significant financial and social pressure on governments, local institutions and families.

Since the combination of surgery with radiation and chemotherapy in the first half of the 20th century, tremendous advances have been made in the treatment of cancer, leading to an improvement in the life expectancy of those affected by it. Early progress was made with the invention of drugs such as methotrexate,[2] liposomal therapy,[3] and combination chemotherapy. More recent therapeutic successes are represented by temozolomide,[4] which in combination with radiotherapy is the first-line treatment for glioblastoma multiforme, an aggressive form of brain cancer; targeting immunotherapeutics such as rituximab[5] and trastuzumab;[6] growth signal inhibitors (e.g., gefitinib, imatinib, and cetuximab); angiogenesis inhibitors (e.g., bevicizumab) and apoptosis-inducing drugs.

The advent of new technologies may have an impact on the way cancer is diagnosed and treated by addressing: 1) the identification of specific biomarkers and development of reliable diagnostic tools for the early detection of cancer as well as monitoring of cancer recurrence; 2) the development of cheap, fast, non-invasive, but at the same time specific and sensitive screening technologies to implement successful cancer screening programs; 3) the development of fast and reliable biopsy tissue diagnosis techniques; 4) the development of agents to facilitate imaging of tumors at both pre- and postangiogenic stage, in all areas of the body; 5) the development of cancer imaging agents specifically engineered to support intra-operative procedures and allow complete removal of solid cancers and their metastases; 6) the engineering of composite materials with powerful anticancer activity which can be selectively and effectively delivered to the tumor site, with consequent reduction of associated side effects.

Advances in nanomaterials science have provided new means with which to tackle cancer-related challenges. Control over the synthesis of inorganic materials at the nanoscale, coupled with improved techniques for nanomaterial surface functionalization, has led to the development of novel functional nanoparticle (NP)-based systems with potential medical applications. Presently, it is possible to synthesize NPs with highly controlled size, shape, morphology, charge, surface chemistry, and physicochemical properties. For in vivo applications, precise control over these parameters is paramount if biocompatible NPs with the ability to overcome biological and physical barriers, such as the immune-system cellular response, liver, spleen, and kidney clearance, high interstitial pressure, and low vascular pressure, are to be engineered. Achieving such control is a heavy focus in the design of systems which can take advantage of, or respond to, specific tumor physiological features, and achieving this control is also critical for the design of therapeutics able to penetrate the cell nuclear membrane.[7] The use of NPs could inspire new routes towards tumor diagnosis, imaging, targeting, drug release and anticancer therapy. Additionally, inorganic NPs offer great potential as a component within multifunctional therapeutics.[8] This review will focus on recent advances in the use of inorganic NPs for cancer-related applications. We will not cover the field of purely organic NPs and refer the reader to excellent reviews on this topic.[9,10,11]

1.1. Exploiting Aspects of Cancer Physiology in Treatment

The term 'cancer' identifies a large group of complex and multifaceted diseases that are characterized by cells that have undergone mutations of their genetic material and whose growth is unregulated. In contrast to benign tumors, cancer cells invade other tissues and spread to other parts of the body through the lymph or the cardiovascular system or both (metastasis). Some specific aspects of nanoscale-materials make them suitable candidates for advancing current technologies with the aim of developing highly sophisticated and effective diagnostic and therapeutic systems for cancer. However, a coherent strategy for the engineering of such systems requires a deep understanding of cancer biology. Important aspects of cancer biology that have inspired the development of specific cancer diagnostic and therapeutic strategies are outlined below.[12]

1.1.1. Defective Vasculature in Tumors

Cancer cells tend to replicate at a higher rate than normal cells. The rapid tumor growth at its early stages of development leads to a lack of nutrient supply to its inner cells, which causes cell death. In order to grow beyond the diffusion-limited maximal size (around 2 mm^3)[13] tumors develop their own vasculature. This 'angiogenic switch' is initiated by local hypoxic conditions inside the tumor resulting in the expression of growth factors such as vascular endothelial growth factor (VEGF) that stimulate the growth of endothelial cells.[14] However, this process is carried out in an accelerated and disorderly fashion, and the resulting blood vessels are tortuous and leaky, lacking in a competent smooth-muscle layer and with irregular diameter (**Figure 1**). The defective vasculature architecture of tumor blood vessels is thought to enhance the extravasation of high molecular weight polymers, proteins, liposomes and particles circulating in the bloodstream, with the low or absent lymphatic drainage then being responsible for their retention at the tumor site. The ensemble of these two processes is often referred to as an "enhanced permeability and retention (EPR) effect" of

Dr. C. Minelli, S. B. Lowe, Prof. M. M. Stevens
Department of Materials & Institute of Biomedical Engineering
Imperial College London
Prince Consort Road, SW7 2AZ London, UK
E-mail: m.stevens@imperial.ac.uk

DOI: 10.1002/smll.201000523

the tumor vasculature.[15] This effect, though not universally accepted, has been described as particularly relevant for particles with diameters from around 60 to 400 nm[16] and will depend on tumor type and stage. Inspired by the EPR effect, many passive targeting strategies have been applied to deliver nanoscale drugs, therapeutics and imaging contrast enhancers to the tumor site, in which such agents are injected into the blood stream with the aim of accumulating preferentially at the tumor site.

The structural and functional abnormalities in tumor vasculature also contribute to the establishment of oxygen gradients in tumours. For example, hypoxic areas away from the O_2 supply can exhibit oxygen tensions as low as 2.5 mmHg (normal tissue: typically 40–70 mmHg).[17] Widespread hypoxia in solid tumors is thought to enhance the progression and aggressiveness of malignant tumors and to be responsible for the low efficacy of radio-, photodynamic- and some forms of chemo-therapy.

1.1.2. pH Gradients in Tumor Cells

Normal cells metabolize glucose under aerobic conditions (exchange of O_2 and CO_2 across the cell membrane). The resulting intracellular pH is about 7.2, while the typical extracellular pH is 7.4. In contrast, tumor cells have elevated metabolic activity and thus exhibit a high glycolysis rate both in aerobic and anaerobic conditions. In addition, the supply of O_2 through the tumor vasculature is poor, as is the removal of CO_2. The combination of these two effects reverses the normal pH gradient found in cells. While the intracellular pH remains at about 7.2–7.3, the extracellular environment in tumours is generally more acidic, with the extent of acidification determined by tumor type.[18,19] Functional nanocarriers have been engineered to respond to the drop in pH between blood vessels (pH 7.4) and the tumor interstitial fluids (Figure 1).[20]

1.1.3. Expression of Biomarkers

Cancer cells may be distinguished from normal cells by their unregulated proliferation and the resulting over- or under-expression of certain biomolecules or alteration of their genetic material (collectively termed biomarkers). A number of cancer-specific biomarkers have been identified, including prostate specific antigen (PSA) for prostate cancer, human epidermal growth factor receptor 2 (HER2) for breast cancer, and cancer antigen 125 (CA-125) for ovarian cancer. Other biomarkers are generically associated with cancers, for example high levels of platelet-derived growth factor (PDGF) which is a growth factor related to angiogenesis, or associated with the risk of developing cancer, such as DNA single-nucleotide polymorphisms (SNPs).[21,22] Many biomarkers found in tumors are also produced by body tissues under normal conditions, but are present in elevated concentrations when tumors are developing. These biomarkers are the targets of most common tools for tumor diagnosis (Figure 1).

The over-expression of specific biomolecules also provides an additional strategy for the delivery of imaging markers and therapeutics to cancer cells (Figure 1). It is possible to functionalize NPs through conjugation with active recognition moieties (active targeting) in order to improve their cancer cell targeting, retention efficiency and cellular up take, though this modification comes at the expense of added complexity.[23] Among the ligands that have been shown to effectively identify tumor sites are: annexin-V which binds to apoptotic cells;[24] epidermal growth factor (EGF) receptor (EGFR) which is over-expressed in certain tumors;[25,26] hypoxia-inducible factor 1 alpha (HIF-1α), whose over-expression is found to be related to angiogenesis, cell survival, glucose metabolism and invasion;[27] and $\alpha_v\beta3$- and $\alpha_v\beta5$-integrins that are over-expressed in endothelial cells within angiogenic blood vessels. Other markers for tumor angiogenesis[28] include aminopeptidase N (APN), VEGF

Having received her Laurea in Physics from the University of Florence (Italy) in 2000, **Caterina Minelli** was PhD student in the Nanoscale Technology & Biochemical Sensing group at CSEM SA (Switzerland). After receiving her PhD in Nanotechnology from EPFL (Switzerland) in 2004, she worked at NIMS (Japan) where she investigated blood interaction with nano-structured materials. In 2007 she was awarded the competitive Marie Curie Fellowship to do research at Imperial College London (UK) in the group of Prof. M. Stevens. Here, she developed engineered biomaterials for cancer therapy and diagnostics, making use of rationally designed peptides and inorganic nanoparticles. Dr. Minelli currently works at NPL (UK).

Stuart Lowe read for a Masters in Physics at the University of Oxford (2004–2008), spending a short time researching the evolution of modular structures using genetic algorithms in the group of Dr. Ard Louis, before joining the group of Prof. Stevens (Imperial College London) as a PhD student. He is currently involved in the development of sensors for the evaluation of enzyme activity using peptide-conjugated quantum dot nanoparticles. Research interests include multiplexed biomarker detection, kinases, proteases, and histone acetyltransferases.

Molly Stevens is Professor of Biomedical Materials and Regenerative Medicine and Research Director for Biomedical Material Sciences in the Institute of Biomedical Engineering at Imperial College London. She joined Imperial in 2004 after a postdoctoral position with Prof. R. Langer at MIT (USA). Prior to this, she graduated from Bath University (UK) in Pharmaceutical Sciences and was awarded a PhD in Biophysics from the University of Nottingham (UK) in 2000. She has been recognized by the TR100, a compilation of the top innovators, under 35, who are transforming technology. Prof. Stevens is developing novel biomaterials-based approaches to tissue engineering and new dynamic nanomaterials, biosensors and drug delivery systems based on specific biomolecular recognition and self-assembly mechanisms.

small NANO MICRO

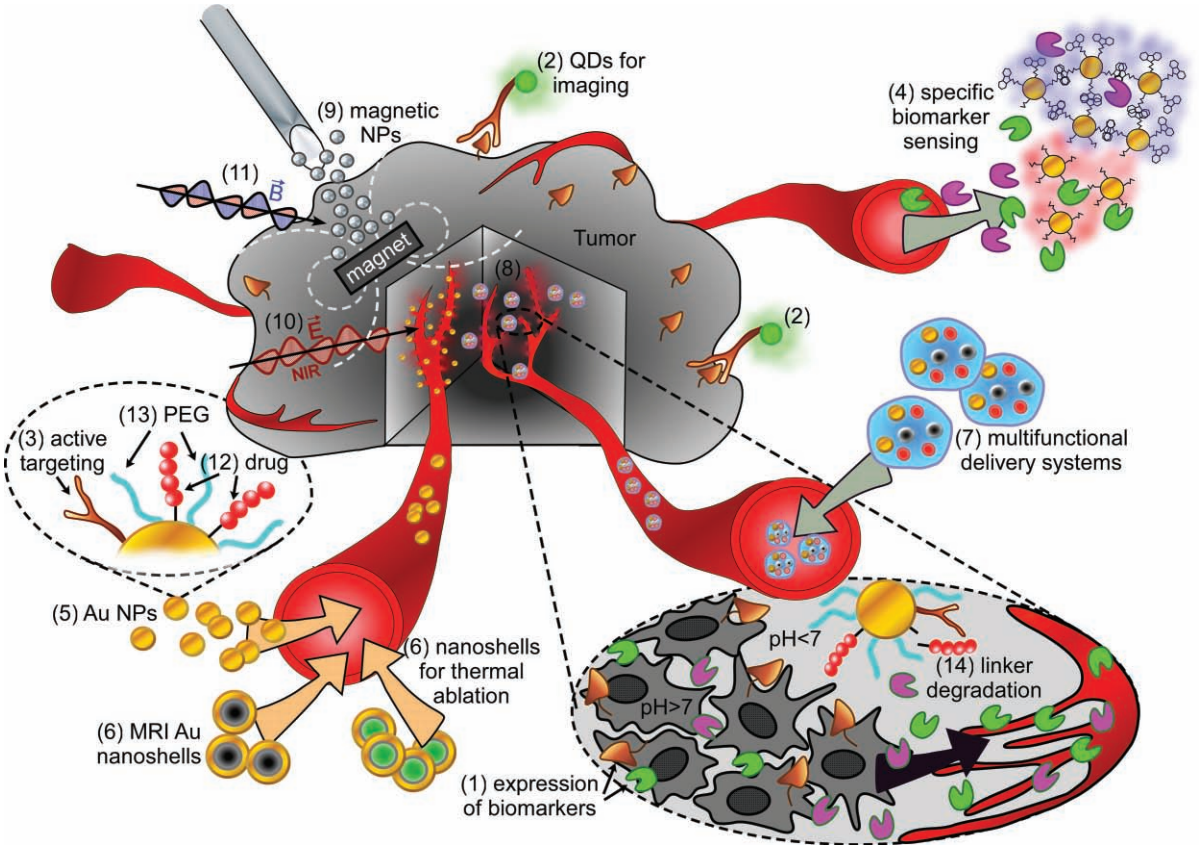

Figure 1. Nanomaterial-based strategies for tumor diagnosis, imaging, and therapy. Tumor cells may over-express biomarkers (1) that can be used as anchoring points to direct the binding of NPs used for labelling (2), imaging, or drug delivery (3). Some biomarkers may be released into the bloodstream, from where they can be detected using NP-based systems (4). Gold NPs (5), composite NPs (6), and multifunctional delivery systems (7) circulating in the bloodstream accumulate in tumors (8). Alternatively, magnetic NPs can be directed into the tumor by means of magnetic fields (9). Engineered NPs can act as heat sources when irradiated, for example, with NIR light (10) and magnetic fields (11), causing tumor cell death. NPs can also be used to deliver drugs and image contrast agents into the tumor (12). NP surface PEGylation is commonly used to improve NP circulation time in blood (13). Drug release can be triggered by environmental factors, such as the acidic pH found in tumor cells (14).

receptors, ephrin type-A receptor 2 (EPHA2), endoglin, and matrix metalloproteinases.

1.2. Physical Properties of Inorganic NPs

Specific aspects of cancer physiology can thus inspire effective strategies to deliver nanoscale therapeutics into tumors, as well as to inform the biomolecular decoration of inorganic NPs. This is oftentimes facilitated by the fact that NPs and biomolecules share the same size range. Materials within this nanoscale size range can possess unique physical and chemical properties not present in the bulk material. These properties arise from the spatial confinement of electrons and from a high surface to volume atom ratio. Some of the nanomaterials used in the treatment of cancer and the physical properties that make them suitable for this purpose are outlined below.

1.2.1. Surface Plasmon Resonance of Metallic NPs

Colloidal metal NPs are a popular material for use in biosensors due to their size-dependent light-scattering properties, first explained theoretically by Mie in 1908.[29] In the bulk form, due to resonance between the oscillating electric field of light and the free electrons in a metal (excitation of surface plasmons), energy is absorbed from incident radiation at a wide range of frequencies. For a NP whose diameter is much smaller than the wavelength of incident light, the free electrons oscillate coherently with the electromagnetic field and resonant states can be induced at precise frequencies. The number of plasmon resonance states is limited by the particle size and geometry, and particles exhibit a strong enhancement of absorption at well-defined surface plasmon resonance (SPR) frequencies (**Figure 2**A).[30,31] The SPR properties of a NP also depend on the local refractive index of the surrounding medium.

A further prediction of the Mie's theory is that plasmon coupling can occur at small inter-particle distances. As a result, aggregates of NPs will have an absorption spectrum where the SPR frequency has been red-shifted (as though the aggregate were a single large particle). Due to the often relatively uncontrolled assembly leading to their formation, NP aggregates will be more polydisperse than the original colloidal sample and hence peak broadening will also occur to some extent.

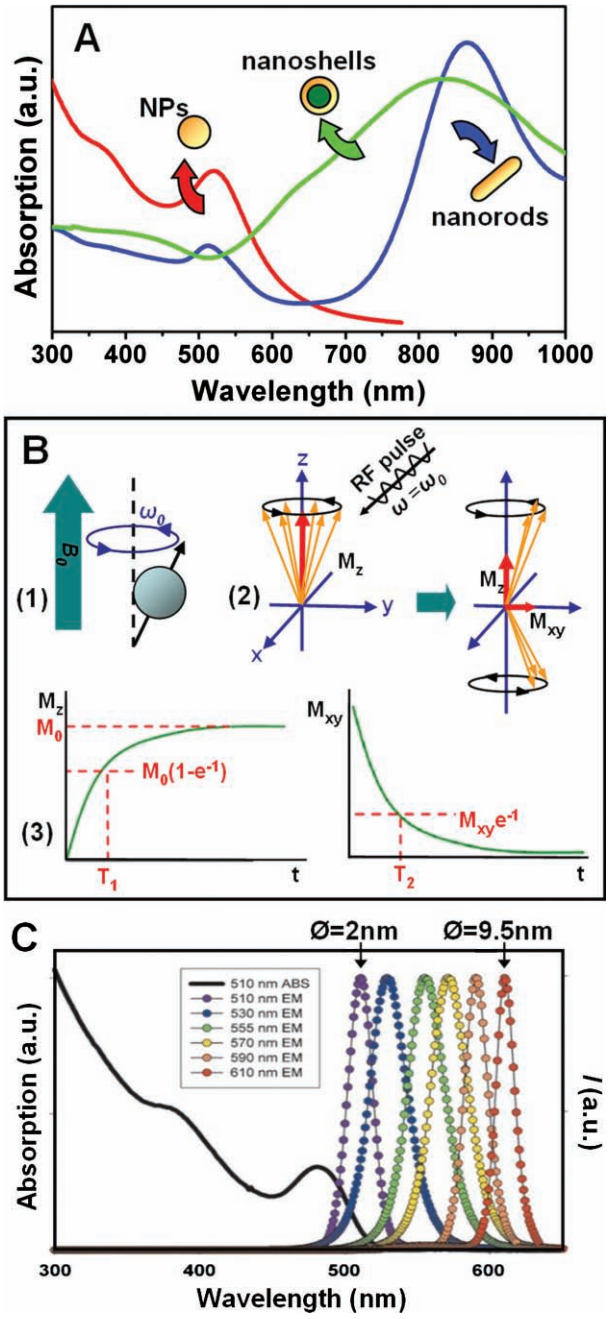

Figure 2. A) Spectral characteristics of gold NPs, nanoshells, and nanorods. B) Principles of MRI. 1) When the protons in atomic nuclei are exposed to a strong magnetic field B_0, their magnetic spins align parallel or antiparallel to the direction of the magnetic field and precess at the Larmor frequency ω_0. 2) When a radio-frequency (RF) pulse is applied, protons absorb energy and are excited. 3) After the disappearance of the RF pulse, the excited protons relax to their initial, lower-energy state and the longitudinal and in-plane moment amplitudes (M_z and M_{xy}) relax back to their initial values with relaxation times T_1 and T_2 respectively. Paramagnetic complexes are usually T_1 contrast agents, while iron oxide NPs are T_2 agents. Adapted with permission.[32] C) Absorption (ABS, solid black line) and emission (EM, circles) spectra of CdSe/ZnS QDs with six different radii. The black line shows the representative absorption of the QDs that emit at 510 nm. Multiple QD emission can be achieved with the same excitation source. Adapted with permission.[33]

With modern synthetic techniques, it is possible to precisely tune the optical properties of NPs in order to adapt them to specific applications. For example, noble metals such as Au, Ag, and Cu have particularly attractive optical properties for the development of colorimetric diagnostic tools, as their SPR frequencies fall within the visible spectrum of light. Furthermore, biological tissue has a minimum in light absorption in the near infrared (NIR) regime (800–1200 nm), making this the optimal range for light penetration with minimal thermal damage.[34] This spectral region is accessible for certain particle geometries.

1.2.2. Photothermal Properties of Metallic NPs

The mechanism of photon-to-thermal energy conversion is the nonradiative decay of free electrons from a photonically excited energy state to the ground state. This energy is dissipated as heat, and the rate of heat transfer becomes particularly large when the NPs are excited at their SPR frequency.[35] In the simple case of a metal nanosphere, the temperature increase in the surrounding medium is modulated as a function of $1/r$, where r is the distance from the NP surface. This means that the highest temperatures, which for example cause the most damage to surrounding biological tissues, are localized in the vicinity of the NPs.

1.2.3. Magnetic NPs

Magnetic NPs have found multiple applications in cancer therapy such as, for example, magnetic resonance imaging (MRI) contrast enhancers (Figure 2B).[32,36,37] The choice of magnetic materials for in vivo use of NPs is restricted by the requirement of biocompatibility and in most studies to date, iron oxide NPs (Fe_3O_4 and γ-Fe_2O_3) have been used. Superparamagnetic NPs are receiving increasing attention for in vivo medical applications. These particles become strongly magnetic when placed in a magnetic field, but their magnetization is lost once the field is removed. As a consequence, these NPs have little tendency to aggregate due to magnetic dipole–dipole interactions (especially if their magnetic core is shell-protected), thus decreasing the risks of embolism.

When magnetic NPs are exposed to an oscillating magnetic field, magnetic energy is dissipated as thermal energy through two distinct mechanisms as the particle returns to its equilibrium state. Brownian relaxation describes the dissipation associated with friction losses due to rotation of a NP in the surrounding medium, while Néel relaxation is related to the rotation of the magnetic moments within the NP magnetic core. When NPs are inside biological tissue, the contribution of Brownian relaxation to heat generation can be hindered by the relatively high viscosity of the medium surrounding the particle.[38] For hyperthermia applications, NP designs that maximize the heat released through the Néel mechanism are therefore favored. Aside from increasing the strength and frequency of the applied magnetic field, the heat generated could potentially be increased by optimizing parameters such as NP size, shape and material, as well as grain structure (which can affect hysteresis properties such as remanence and coercivity).[39] Furthermore, monodisperse NP samples have the highest associated energy transfer.[40]

small NANO MICRO

NP concentration critically affects the local temperature increase that can be achieved through magnetic heating and for this reason magnetic NPs are usually injected locally into tumors.

1.2.4. Optical Properties of Luminescent Quantum Dots

Recombinant fluorescent proteins or organic fluorophores are frequently used for biomarker sensing or labeling. Recently, there has been an increasing interest in the use of inorganic semiconductor nanocrystals, known as quantum dots (QDs), in biomedical applications due to their unique optical properties.[41–43] The size of the QDs leads to quantum confinement of excitons, meaning that the electron valence and conduction bands are no longer a continuum, but rather are split into discrete energy levels. Upon photoexcitation, an electron–hole pair is created and releases a photon of specific energy upon recombination. The energy gap corresponding to the transition between the excited and the ground states is size- and material-dependent, and in the case of materials such as CdSe, CdS, among others, the transition produces photons in the visible spectrum. QDs have attractive optical properties such as tunable emission wavelength[44] and resistance to photobleaching.[45] QDs also have strong absorbance at a wide range of wavelengths far from the emission peak allowing for effective filtering of excitation radiation without affecting the emission detection. Hence, multiple QDs with different sizes and therefore different emission wavelengths can be excited with a single source (Figure 2C). Excitation of multiple wavelengths in this way is more difficult to achieve using conventional fluorescent molecules with narrow, non-overlapping absorption bands. By exploiting these optical properties of QDs, systems that can simultaneously detect or image multiple unique targets with a single monochromatic excitation source have been developed.[46–49] For example, **Figure 3**A illustrates a QD-based assay theoretically capable of coding one million nucleic acid or protein sequences.[49]

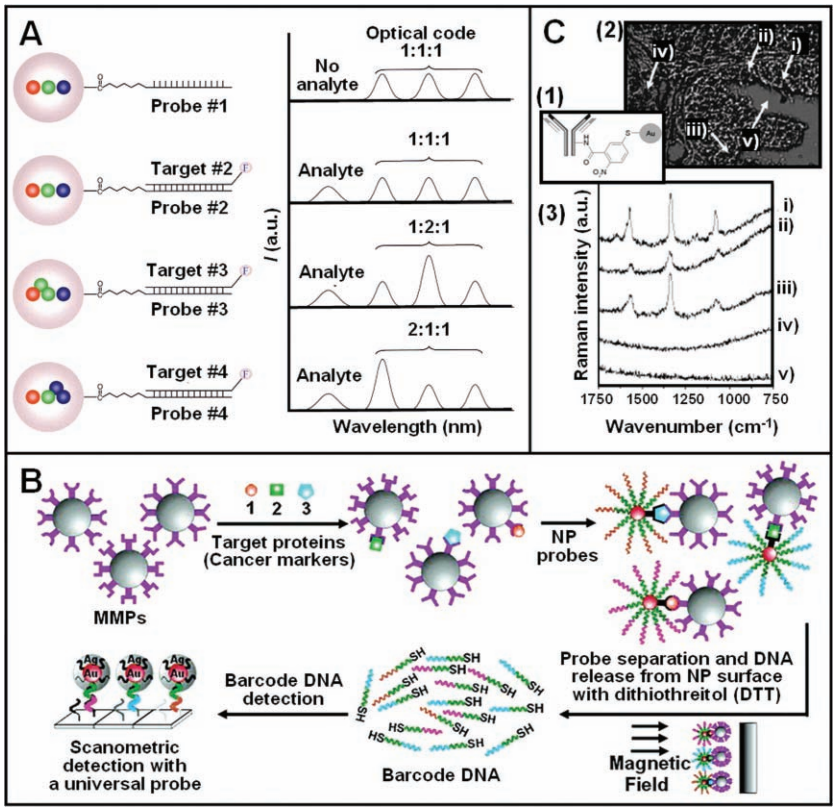

Figure 3. A) Schematic illustration of multiplexed DNA hybridization assays using QD-tagged beads. Streptavidin-coated 1.2 μm polymer beads are loaded with differing ratios of CdSe/ZnS core/shell QDs. Biotinylated probe oligonucleotides are conjugated to the beads by biotin-avidin linkage, while target oligonucleotides are labeled with a blue fluorescent dye. Target binding is detected by observing the dye peak alongside the bead spectrum, which identifies the target sequence (graphs to the right). The use of 10 intensity levels and 6 colors could theoretically code one million nucleic acid or protein sequences. Reprinted with permission.[49] Copyright 2001, Macmillan Publishers Ltd: Nature Biotechnology. B) Example of multiplexed and amplified detection, where magnetic and gold particles are used in a sandwich assay to detect multiple cancer markers in solution. 30 nm gold NPs are co-loaded with polyclonal antibodies and ssDNA sequences comprising universal and specific (barcode) portions. The "barcodes" are used to uniquely identify each different antibody. Magnetic microparticles (MMPs) are each functionalized with one type of monoclonal antibody corresponding to the same targets as the gold NP probes and passivated with BSA. The MMPs are incubated with a number of different cancer targets. Upon gold NP probe addition, MMP-analyte-gold NP sandwiches form. A magnetic field is then used to separate bound gold NPs from the unbound. Subsequently the barcode DNA is released from the bound gold NPs and transferred to a complementary DNA array for detection. Notably, for each bound analyte multiple barcodes are released enabling signal amplification. The barcodes bind the chip surface through their specific sequence, and the chip is read using gold NPs functionalized with ssDNA complementary to the universal sequence. Adapted with permission.[50] Copyright 2006, American Chemical Society. C) Immuno-Raman spectroscopy for labeling and imaging of specific receptors. 1) Structural formula of the PSA immunolabel. 2) White light microscope image of epithelial tissue from the prostate and 3) Raman spectra recorded in situ at the locations indicated by arrows; i–iii) epithelium, iv) stroma, v) lumen. The Raman signal is enhanced due to interaction with the enhanced electric field at the gold NP surface (SERS). The anti-PSA SERS label is present only at positions (i–iii). Adapted with permission.[51]

QDs can also act as efficient donors in Förster resonance energy transfer (FRET)[52–56] and as energy acceptors in bioluminescence resonance energy transfer with a bioluminescent protein.[57] Gold NP–QD systems have attracted significant interest in biosensing because gold NPs have a higher quenching efficiency and larger Förster radius than traditional organic FRET acceptors.[58] Alternatively, metal complexes have also been used for nonradiative energy transfer and hence distance-dependent loss of QD photoluminescence (PL), their oxidation states having energy levels slightly displaced from the surface states of QDs.[55]

2. Cancer Diagnosis

Current methods for cancer diagnosis focus on the morphological evaluation of tissue sections, and patients may only be diagnosed with cancer after they have sought medical attention for symptoms related to their tumor. This limitation often delays cancer detection until quite a late stage, increasing the chance that the cancer has metastasized to other organs. Hence, the accurate diagnosis of cancer in its earliest stages is of extreme clinical importance. Indeed, early tumor diagnosis is nowadays recognized as a key priority in the UK and World Health Organization cancer strategies.[59,60]

A number of highly sensitive biomarker detection systems utilizing the physical properties of inorganic NPs have been designed. **Table 1** lists some examples which we have organized by medical application. Below, we also review some of the systems applied to specific classes of cancer biomarkers, as well as discuss some detection modalities that are particularly effective when used in conjunction with nanomaterials.

2.1. NP-Inspired Strategies for Cancer Diagnosis

In addition to the properties of NPs previously discussed, there are three aspects of NP-based systems that can specifically impact diagnostics for cancer, namely multiplexed detection, miniaturization and signal enhancement.

The functionalization of independent populations of NPs with different biomarker-responsive molecules offers a strategy for the simultaneous detection of a set of signals. This multiplexed detection capability is particularly attractive for complex diseases such as cancer, where simultaneous information from a range of biomarkers can provide a more accurate diagnosis. Several examples of use in NP-based assays will be presented.[46–48,55,58,61] One highly sensitive NP-based multiplexed system that has found successful clinical application is the bio-barcode system developed by the Mirkin group (Figure 3B).[62,63] This technology, now commercialized with the Verigene system from Nanosphere, Inc. was approved by the US Food and Drug Administration (FDA) in 2007.

The use of NPs potentially allows for device miniaturization, while retaining a large surface area available for sensing. Other consequences of miniaturization include integration of NP-based detection systems with the lab-on-a-chip approach, furthering the development of cost effective point-of-care devices with rapid response and low sample volume consumption.

Increased detection sensitivity has been achieved by combining the use of NPs with detection systems typically used for molecular analysis and imaging, such as, for example, surface enhanced Raman scattering (SERS, see Figure 3C).[51,64] NP-coated electrochemical sensors have also shown remarkable sensitivity in conjunction with signal-amplifying bioconjugated magnetic NPs.[65] A high total surface area available for molecular binding on NPs is certainly responsible for increased detection sensitivity. However, in many cases the exact mechanism of signal enhancement is not yet fully understood. The use of techniques relying on the signal-enhancing properties of NPs for biomolecule detection is still relatively uncommon and requires specialized equipment, but further research promises to yield rapid-response, high-sensitivity detection platforms.

2.2. Detection of Single-Nucleotide Polymorphisms (SNPs)

SNPs are mutations that involve the alteration (substitution, deletion, or insertion) of a single base in the genetic code. The identification of cancer-specific SNPs would give a useful indicator of a person's predisposition to the disease. However, routine, low-cost, personalized screens for SNPs will only become accessible with increased assay detection sensitivity, allowing for rapid screening and reduced sample and reagent use. To this end, a number of NP-based strategies for SNP detection have been developed. The strong emission and narrow linewidth of QD spectral peaks can improve the signal-to-noise ratio in genetic screens, decreasing both sample consumption and assay duration. For example, as illustrated in **Figure 4**A QDs enable discrimination between SNP variants of the cancer gene p53 within 10 minutes of analyte introduction.[66] Gold NP-DNA conjugates capable of distinguishing between complementary and SNP targets were developed by using a three-strand assembly system and monitoring its melting temperature. Two DNA strands present different sequences which, when arranged contiguously, are complementary to a third, target sequence. In the presence of the target sequence the NPs are thus aggregated. Upon raising the temperature, the stability of the DNA duplex is disrupted, the gold NPs redisperse and the NP solution color changes from blue to pink.[67] The assay format was further developed by introducing high-fidelity ligase enzymes to stabilize complementary sequences against melting, whereas sequences containing a SNP at the ligation site remained unstable.[68]

2.3. Detection of Tumor-Related Antigens

The detection of biomarkers provides information not only about the presence of cancer, but also on its phenotype and propensity to metastasize, and therefore has an important role in the choice of the course of treatment. For this reason, numerous biomarker assays have been developed, with particular emphasis on prostate and breast cancer, which are the most common types of cancers found in men and women respectively. PSA is one of the most commonly investigated cancer biomarkers, as it can indicate the presence of prostate cancer when expressed at elevated levels (i.e., >4.0 ng mL^{-1}[71]). The typical sensitivity of clinically employed enzyme-linked immunosorbent assay (ELISA) for human PSA is 0.1 ng mL^{-1}, which is well within the required sensitivity range. However, much higher detection sensitivity is required for monitoring of prostate cancer recurrence in men who have had their prostate removed (i.e., approximately picogram per milliliter).[72] NP-based immunoassay systems capable of measuring clinically relevant PSA levels have been developed using both gold NPs[62,73–75] and QDs.[76]

small NANO MICRO

Table 1. Nanomaterials used in the diagnosis of cancer. For each application, we provide details of the nanomaterials functionalization strategy, the medium used to test the assay, as well as the physical properties of the nanomaterials on which the assay is based.

Application	Nanomaterial	Conjugate	Detection medium	Physical property	Reference
SNP detection	Gold NPs	ssDNA	Buffer	SPR blueshift with NP dispersion	[67,68]
SNP detection	QDs	ssDNA	Buffer	Photoluminescence	[61,66]
PSA detection (prostate cancer)	Gold NPs	Antibody	Serum	SERS	[64]
PSA detection (prostate cancer)	Gold NPs	Antibody	Buffer	SERS	[51]
PSA detection (prostate cancer)	Gold NPs	Designer peptides	Buffer	SPR blueshift with NP dispersion	[73]
PSA detection (prostate cancer)	Gold NPs and gold nanorods	Antibody	Buffer	Scattering	[75]
PSA detection (prostate cancer)	Gold NPs and magnetic microparticles	Antibody	Serum, cell lysate	NP-coated electrode surface area	[65]
PSA detection (prostate cancer)	Gold NPs and magnetic microparticles	Antibody and ssDNA	Buffer, serum	Magnetic separation, high surface area	[50,62,72]
PSA detection (prostate cancer)	QDs	Streptavidin	Serum	Photoluminescence	[76]
Protease detection	Gold NPs	Designer peptides	Buffer	SPR blueshift with NP dispersion	[73]
Protease detection	Gold NPs	Designer peptides	Buffer	SPR blueshift with NP dispersion – SERS	[84]
Protease detection	QD – gold NPs	Designer peptides	Buffer	FRET	[58,85]
Protease detection	QDs	Designer peptide – dye	Buffer	FRET	[54]
Protease detection	QDs	Designer peptide – dye	Buffer, cell culture medium	FRET	[69]
Protease detection	QDs	Designer peptide-bioluminescent protein	Buffer, serum	bioluminescence resonance energy transfer	[57]
Kinase detection	Gold NPs	Designer peptides	Buffer	SPR redshift with NP aggregation	[82]
Kinase detection	Gold NPs	Designer peptides	Cell lysate	SPR redshift with NP aggregation	[95]
Kinase detection	QDs	Designer peptides – dye-labeled antibody	Buffer	FRET	[96]
Biomarker and DNA detection	Gold NPs	Aptamer (for PDGF detection)	Buffer, cell culture medium	Fluorescence quenching	[79]
Biomarker and DNA detection	Gold NPs	Antibody, aptamers, and oligonucleotides	Buffer, serum	Change in NP scattering and Brownian motion upon NP aggregation	[80]
Biomarker and DNA detection	Gold NPs and magnetic microparticles	Antibody and ssDNA	Buffer, serum	Magnetic separation, high surface area	[50,62]
Biomarker and DNA detection	Gold NPs and magnetic microparticles	Antibody and ssDNA	Buffer	Magnetic separation, high surface area	[63]
Assessment of presence of cancerous cells in biopsied tissue	Oval-shaped gold NPs	Anti-HER2 and aptamers	Buffer	SPR redshift with NP aggregation	[98]
Assessment of presence of cancerous cells in biopsied tissue	QD coated magnetic microparticles	EGF	Cell culture medium	Magnetic separation and photoluminescence (multifunctional approach)	[99]
Assessment of presence of cancerous cells in biopsied tissue	Cd-free QDs	Anticlaudin 4 and antiprostate stem cell antigen	Cell culture medium	Photoluminescence	[183]

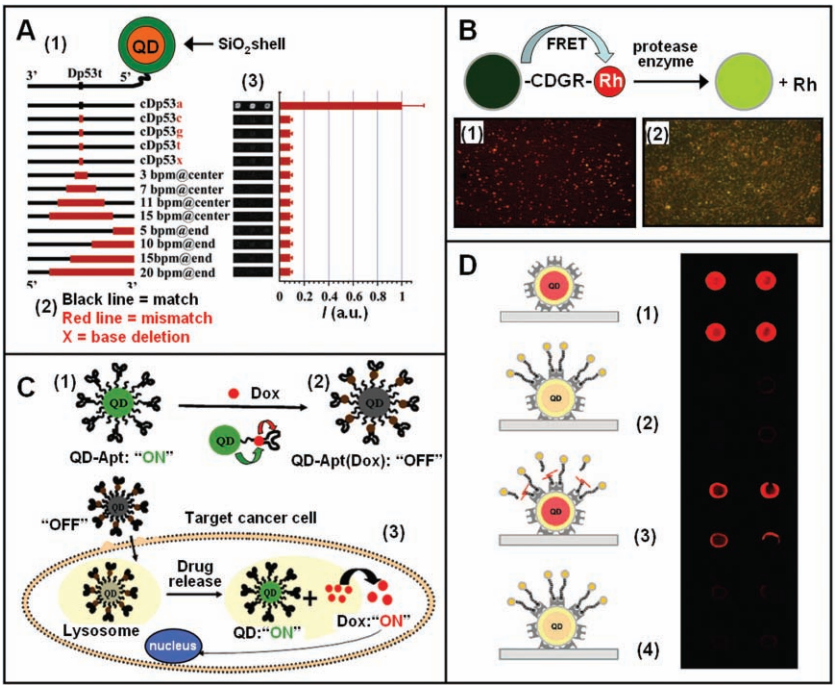

Figure 4. QD-based biomarker detection strategies. A) Human genetic cancer marker p53 SNP assay making use of core/shell CdSe/ZnS QDs. 1) The QDs are embedded in a silica shell and conjugated to a ssDNA sequence labeled Dp53t. 2) Complementary and mismatch sequences are immobilized onto glass slides (spot size 100 μm). cDp53a is the perfect complement sequence. In other sequences base mismatches are introduced either at the center or the 3' end; the 5'-termini are used for DNA immobilization. 3) The probes are incubated on the DNA array, and the emission signal is detected with a commercial fluorescence scanner. Following hybridization, a positive signal is observed only for the cDp53a sequence (signal-to-background ratio of ~12). Reproduced with permission.[66] Copyright 2003, American Chemical Society. B) Protease collagenase-based QD-FRET detection of cancerous cells in culture. Top: Schematic of QD-dye assembly. Rhodamine dye (Rh) is attached to the Arg residue of an RGDC peptide sequence, where the Cys residue binds CdSe/ZnS core/shell QDs. In this conformation, the QD green emission at 545 nm is quenched, while the Rh red emission at 590 nm is enhanced by FRET. In the presence of collagenase enzyme, the peptide is cleaved and the PL emission of the QDs is recovered. Bottom: fluorescence microscopy images of 1) normal and 2) breast cancer cells incubated with the Rh-labeled peptide-coated QDs for 15 min. In image (1) the red emission is due to Rh, while in (2) the QD emission is detected due to the presence of collagenase (over-expressed by breast cancer cells), which cleaves the peptide sequence. Adapted with permission.[69] Copyright 2006, American Chemical Society. C) Monitoring of intracellular drug release. 1) CdSe/ZnS core-shell QDs are functionalized with an RNA aptamer which recognizes the extracellular domain of prostate specific membrane antigen. The QD-aptamer conjugates exhibit luminescence ("ON" state). 2) Intercalation of the drug molecule doxorubicin (Dox) quenches the QD luminescence, while the Dox fluorescence is in turn quenched by the aptamer ("OFF" state). 3) Cell targeting and drug release. Intercalation of Dox with the aptamer does not alter its selectivity for prostate cancer cells and the QD-Aptamer-Dox conjugates are internalized into lysosomes by receptor-mediated endocytosis. Gradual release of Dox and its subsequent escape from the lysosomes causes the recovery of QD fluorescence, providing a means to measure intracellular Dox release, as well as to perform cell imaging. Adapted with permission.[70] Copyright 2007, American Chemical Society. D) Chip-based assay for matrix metalloproteinase MMP-7 and its inhibitors by using CdSe QD-gold NP conjugates. 1) Streptavidin-coated QDs are arrayed directly onto a glass surface and their PL emission is detected. 2) Gold NPs are mono-conjugated with biotinylated designer peptide, susceptible to cleavage by MMP-7. The biotin group binds strongly to the streptavidin at the QD surface, causing the quenching of the QD emission due to the close proximity of the gold NPs. 3) Following introduction of MMP-7, the peptide is cleaved, leading to recovery of QD luminescence. 4) In the presence of MMP-7 inhibitors, the peptide cleavage is prevented and the QD emission signal remains quenched. Adapted with permission.[58] Copyright 2008, American Chemical Society.

Grubisha and co-workers[64] reported a SERS-based assay using gold NPs, with a PSA detection limit of 1 pg mL^{-1} in human serum. The gold NP bio-barcode developed by Mirkin's group (Figure 3B) has achieved the detection limit of 330 fg mL^{-1} PSA. The sensitivity of this detection system has enabled the monitoring of very early prostate cancer recurrence in men who have had their prostate removed and hence predict disease prognosis.[62,74] Importantly, the bio-barcode system is also capable of multiplexed detection: simultaneous detection of PSA, human chorionic gonadotropin and α-fetoprotein has been achieved by using this system.[50] At higher concentrations, for example the 4.0–10.0 ng mL^{-1} range, which is a diagnostic grey area for prostate cancer,[71] this technique could greatly impact the accuracy of the diagnosis. A more accurate diagnosis can be formulated by measuring the percentage of free PSA (not complexed to protease inhibitors)[77] or a cocktail of biomarkers.

An innovative approach to the detection of biomarkers is based on FRET occurring between aptamer-functionalized gold NPs and fluorophores.[78] **Figure 5**A illustrates such an assay for the detection of the breast cancer.[79] An aptamer-binding method based on single gold NP counting for the detection of carcinoembryonic antigen (CEA) and alpha fetal protein (AFP) has also been demonstrated.[80]

2.3.1. Detection of Enzyme Activity

Protein-modifying enzymes play a large part in cellular processes such as signaling pathways and the cell growth cycle. A developing cancer can cause their overexpression or result in atypical enzyme activity and for this reason it is clinically important to develop techniques able to detect not only the concentration but also the activity of such enzymes. One such enzyme family is the proteases, which can recognize and cleave specific amino acid sequences. PSA is an example of a protease which has an important role as a cancer biomarker (see above), as well as matrix metalloproteinases, which have been implicated in cancer progression, including metastasis.[83] ELISA cannot distinguish between the latent and active form of an enzyme. In contrast, a variety of protease assays based on the cleavage and dispersion of a peptide-crosslinked

small NANO MICRO

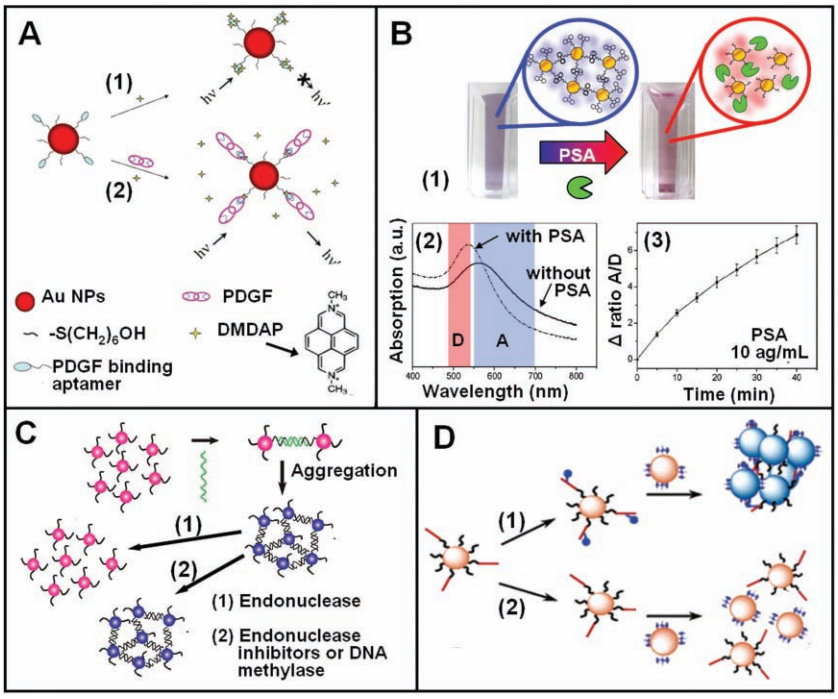

Figure 5. Gold NP-based biomarker detection strategies. A) Schematic representations of aptamer-functionalized gold NPs for the detection of platelet-derived growth factor (PDGF). The aptamer has a unique structure that allows binding of both PDGF and the fluorophore dimethyldiazapyrenium (DMDAP). 1) The fluorescence of DMDAP is almost completely quenched by the NPs when it is intercalated with the aptamer. 2) The fluorescence is restored upon PDGF-aptamer binding and displacement of DMDAP. Adapted with permission.[79] Copyright 2007, American Chemical Society. B) Colorimetric assay for protease detection. 1) Gold NPs are functionalized with rationally designed peptides containing a PSA-specific cleavage sequence and terminated with a Cys residue for NP binding. An N-terminal Fmoc group enables NP assembly by π–π stacking interactions with Fmoc groups on neighboring NPs. Introduction of PSA enzyme leads to peptide cleavage and consequent particle dispersion, which causes NP solution to change color from blue to pink. The NP acquires a positive charge upon enzymatic cleavage, thus stabilizing the NP dispersion by electrostatic repulsion. 2) SPR peak of the gold NPs before and after protease addition. The peak blue-shift is quantified by computing the A/D ratio, where A and D are the areas under the spectral curves between 490 and 540 nm (red), and 550 and 700 nm (blue) respectively. 3) A/D ratio variation vs. time upon 10 ag/mL PSA addition. Adapted with permission.[73] Copyright 2007, American Chemical Society. C) Schematic of gold NP-based assay for endonuclease and DNA methylase activity and their inhibitors. A single population of DNA-functionalized gold NPs is crosslinked by an endonuclease-specific substrate strand, causing the NP solution to change color from pink to blue. 1) In the presence of the specific endonuclease, the substrate is cleaved and the gold NPs are dispersed, returning the solution to a pink color. 2) The pre-addition of endonuclease inhibitors such as DNA methylases prevents endonuclease-mediated cleavage, resulting in the solution remaining blue in color. Adapted with permission.[81] Copyright 2009, American Chemical Society. D) Gold NP-based assay for kinase detection and inhibitor screening. Gold NPs coated with a mixed peptide layer consisting of a stabilizing peptide and a kinase-specific substrate peptide are incubated with kinase enzyme and biotin-modified ATP, thus appending a biotin molecule to the substrate peptide. Streptavidin-coated gold NPs are then added resulting in NP aggregation by biotin-avidin binding. The aggregation state and resulting SPR peak shift is dependent on inhibitor concentration: 1) no inhibitor, 2) inhibitor saturation. Adapted with permission.[82] Copyright 2006, American Chemical Society.

NP assembly have been developed. Figure 5B illustrates an example of such an assay, which used 10 nm gold NPs to achieve a sensitivity of 10 ag mL^{-1} for PSA detection, with an even higher potential sensitivity demonstrated.[73] As this is the highest published sensitivity for PSA detection, such a system may be very useful for monitoring the relapse of prostate cancer after surgical treatment. This approach was also combined with a SERS technique and demonstrated a potential detection limit in the range of picograms per milliliter of enzyme.[84]

QD-based methods for protease detection tend to rely on PL quenching by a molecule attached to the QD via a protease-cleavable peptide linker. Upon introduction of the enzyme, the quencher molecule is released and the PL signal is recovered. Examples of quencher molecules used are fluorescent dyes[54,69] (Figure 4B,C), gold NPs[58,85] (Figure 4D), and ruthenium metal complex.[86] QD-based bioluminescence resonance energy transfer systems for matrix metalloproteinase detection have also been reported.[57]

DNA repair enzymes play an important role in removing mutations that may enter the genetic code.[87,88] Abnormal activity of DNA exo- and endonucleases can thus lead to an accumulation of mutations, some of which may increase cancer risk (for example, mutant forms of hOgg1 glycosylase have been implicated in increased susceptibility for lung cancer).[89] Restriction endonucleases, which cleave a specific DNA sequence, have been used as a model system for detection of DNA-modifying enzymes. Gold NP aggregation-dispersion systems have been applied for endonuclease detection and inhibitor screening.[81,90,91] Figure 5C shows an example of such a system where a three-strand NP linking strategy is used and where the central strand is an endonuclease-cleavable target.[81] An endonuclease detection assay making use of surface-immobilised gold NPs with single particle resolution was also reported. The enzymes site-specifically cleave the DNA, releasing the NPs out of the focal plane of a dark field microscope.[92]

Protein kinases, which transfer the γ-phosphate from ATP to the hydroxyl group of certain amino acid residues, are heavily involved in cell signaling and cell cycle regulation. Many kinases are the targets of anticancer drugs,[93] with many more touted as potential future targets.[94] Kinase-mediated peptide phosphorylation has been used as the basis of multiple NP-based assays. For example, the γ-phosphate of ATP was modified with biotin to specifically biotinylate phosphorylated peptides and induce aggregation of streptavidin-coated NPs in the presence of enzymes (Figure 5D).[82] Oishi and coworkers[95] developed a similar assay where the aggregation of the peptide-functionalized NPs was triggered by the change in peptide charge upon phosphorylation. This system was used to

detect hyperactivation of protein kinase Cα in the cell lysate of melanoma cells. A QD-based kinase detection assay was also recently developed, where dye-labeled monoclonal antibodies were used to bind to phosphorylated peptide-functionalized QDs, inducing a FRET signal indicating kinase activity.[96,97]

2.4. Morphological Evaluation of Biopsied Tissue

The assessment of a biopsied tissue sample always precedes surgical cancer removal. However, the evaluation of these samples can be lengthy and rapid tests able to reliably assay the presence of cancer cells in tissue samples are highly sought by surgeons. In this regard, Lu and co-workers[98] developed a colorimetric assay based on oval-shaped NPs functionalized with both antibody and aptamers which specifically bind receptor HER2 on breast cancer cell surfaces. The presence of breast cancer cells alongside NPs induces NP aggregation which is then quantified by UV adsorption and two-photon scattering. QD coated magnetic microparticles were also engineered to develop an assay with magnetic/cell targeting properties and optical readout (see **Figure 6**). The NPs were capable of selectively binding cancer cells, which could be rapidly separated from noncancer cells by means of a magnetic field and subsequently detected by fluorescence microscopy.[99] Furthermore, due to their unique optical properties, biomarker-conjugated QDs have the potential to replace common fluorescent labels for cancer cell imaging in tissue specimens.[100]

3. Treatment and Monitoring of Cancerous Tumors

Successful use of NPs in cancer imaging and treatment relies on the uniqueness of NP physical properties and the way these properties are integrated with current technologies for cancer therapy. **Table 2** and **3** list some examples of the use of NPs in cancer imaging and therapy respectively. Some examples will also be described in the following sections.

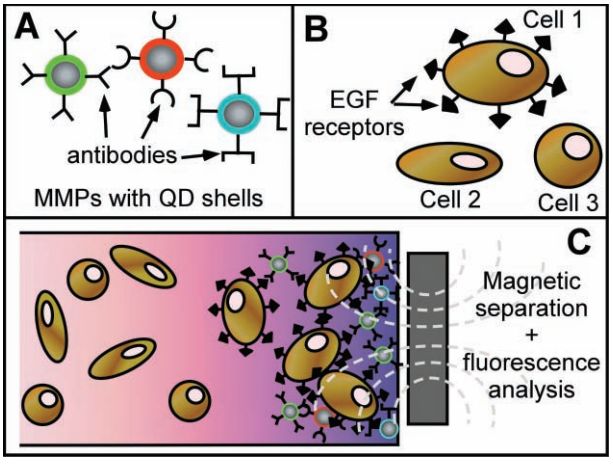

Figure 6. Schematic showing labeling and separation of specific cell types using multifunctional probes. A) CdTe QDs are electrostatically adsorbed onto magnetic polystyrene particles (MPP). Different proteins or antibodies are conjugated onto the QD-coated MPPs, including epidermal growth factor (EGF). B) A suspension of cells from culture is prepared, including breast cancer cells over-expressing EGF receptors. C) QD-coated MPPs bind cancer cells, which can be magnetically separated from the solution and detected.[99]

A major problem arising with the in vivo use of therapeutic agents is that low molecular weight drugs and nontargeted contrast enhancers are rapidly cleared from the body after injection, resulting in limited action and a short time window available for detection. The encapsulation or conjugation of these agents with biocompatible polymers such as poly-ethylene glycol (PEG) and *N*-(2-hydroxypropyl)methacrylamide (HPMA),[10] liposomes[101] and dendrimers[102] has proven to be a successful approach to improving a cancer therapeutic's water solubility, circulation time in the body and tumor uptake, in turn reducing drug payloads and associated toxic effects. PEG, an FDA-approved, nontoxic polymer exhibiting high resistance to protein adsorption, is a particularly popular passivating molecule. PEG molecules are strongly hydrophilic[103] and form a surface-bound highly hydrated layer around the NPs. This layer shields the NPs from interactions with cell surface proteins, thereby limiting NP elimination via the immune system.[23,104,105]

3.1. NPs in Tumor Imaging

Tumor imaging plays a fundamental role in cancer therapy, from informing the diagnosis (and consequent choice of treatment), to the pinpointing of diseased areas during treatments (e.g., radiotherapy), and extending to post-treatment monitoring. Tumor imaging tools are also used successfully in widespread screening programs such as mammography, which is used to detect breast cancers. The primary objective of tumor imaging is to pinpoint tumor location(s) at the earliest possible stage in any part of the body. Current technologies such as MRI allow imaging of solid tumors as small as 1 mm^2 (about 10^6 cells), which corresponds to tumors at the point of the angiogenic switch. However, no technique in clinical practice is currently able to distinguish smaller groups of cancer cells in vivo. Promisingly, the use of QDs in fundamental in vivo studies on tumor metastasis[106] and tumor vasculature[107] has allowed for imaging at unprecedented levels of detail.

Tumor imaging techniques have evolved through historical advances in physics and chemistry and often rely on complex technologies.[108] However, they all share a common conceptual feature: they aim to increase the signal from the tumor with respect to the background. The elevated cell density or level of vascularization present in tumors can, in itself, provide some signal enhancement. The signal-to-noise ratio is further increased by using image contrast enhancers. NP-based imaging systems could provide new means of achieving image contrast and tumor localization.

3.1.1. NPs as Contrast Enhancers

The current status of emerging imaging technologies for cancer applications has been critically reviewed by Frangioni.[109] Here, we will review the use of new nanomaterials

small NANO MICRO

Table 2. Nanomaterials used in the imaging of cancer. For each application, we provide details of the strategy adopted to deliver the nanomaterials to the tumor in in vivo experiments, as well as the physical properties of the nanomaterials used for imaging.

Application	Nanomaterial	In vitro	In vivo	Delivery	Physical property	Reference
Radio-labeling	^{192}Au colloids		√	–	Radioactivity	[113]
MRI marker	Magnetic NPs		√	Intravenous injection Active targeting (anti-HER2)	Magnetism	[111]
	Paramagnetic NPs		√	Active targeting ($\alpha_v\beta_3$-intregrin)	Magnetism	[112]
	Magnetic/Au core/shell NPs		√	Local injection	Magnetism	[110]
	Nanoshells – magnetic NPs	√		Active targeting (anti-HER2)	Magnetism of magnetic NPs	[158,159]
X-ray contrast agents	Gold NPs		√	Intravenous injection	Opaque to X-rays	[114,117]
Spectral-domain optical coherence tomography	Gold NPs		√	Local injection Active targeting (anti-EGFR)	Strong scattering	[115]
Cancer imaging	QDs		√	Intravenous injection Active targeting	Photoluminescence	[106,107]
Raman spectroscopy tags	Gold NPs		√	Intravenous injection Active targeting (anti-EGFR)	Surface Enhanced Raman Scattering	[116]
Early stage therapy monitoring	Gold NPs	√		–	FRET	[118]
Lymph node tracers	QDs		√	Intradermal injection	NIR fluorescence	[120–122]
	Gold nanocages		√	Intradermal injection	SPR in NIR range	[119]

for cancer imaging. However, the use of NPs for MRI has been recently reviewed by Na and co-workers[32] and we refer the reader to their work for in-depth coverage of this topic and to Figure 2B,[32] 7A,[110] 7B[111] for some examples. It is worth mentioning that a NP-based MRI contrast agent developed at the Siteman Center of Cancer Nanotechnology Excellence of Washington University is currently undergoing Phase I clinical trials. The contrast agent binds to $\alpha_v\beta_3$-intregrin, which is over-expressed by angiogenic tumor endothelial cells and is therefore associated with early tumor development.[112]

Colloidal gold has been widely investigated for in vivo medical applications because of its biocompatibility and facile conjugation with biomolecules via thiol, disulfide and amine moieties. For example, radioactive ^{192}Au colloids were used for the radiolabeling of lymph nodes in proximity to mammary tumors as early as the 1950s.[113] Gold NPs have been used as in vivo X-ray contrast enhancers for X-ray computed tomography (CT),[114] spectral-domain optical coherence tomography (SD-OCT),[115] and Raman spectroscopy,[116] while gadolinium chelate-coated gold NPs have been shown to exhibit dual imaging capability by CT and MRI (**Figure 7**C).[117]

The response of solid tumors to therapy is usually monitored by measuring the rate of regression. However, the limited sensitivity of current imaging techniques does not allow monitoring of the early stages of tumor regression. To overcome this limitation, Oishi and co-workers[118] developed a probe with internalized gold NPs sensitive to cell apoptosis (Figure 7D). This system was able to detect apoptotic cells in vitro as early as one day post treatment. Probes based on the same principle are being developed by the same group for in vivo MRI applications.

3.1.2. NPs for Intra-operative Imaging of Cancer Cells

The inspection of sentinel lymph nodes (SLNs) is mainly practiced in breast cancer surgery at present, where SLNs are biopsied to determine whether a cancer has metastasized, but this procedure requires a highly experienced surgeon. The current gold standard for guiding surgery is isosulfan blue dye in combination with radioisotopes localized in the SLNs. However, isosulfan blue suffers from some limitations, including high propensity to photobleach and an emission wavelength that does not penetrate far into soft tissue. Engineered nanoparticles offer a range of solutions which promise to overcome such limitations. For example, gold nanocages absorbing in the NIR region have been used for SLN detection by non-invasive photoacoustic imaging (Figure 7E).[119] The NIR region is particularly attractive since it coincides with a minimum in biological tissue absorption and autofluorescence. NIR-emitting QDs have also proven useful for SLN mapping as the hydrodynamic diameter of the stabilized QD falls within the size range required for retention in the SLNs (5–50 nm).[120–122] Kim and co-workers[120] reported a QD-based SLN labeling procedure where the QD photoluminescence could be detected at a depth of up to 1 cm in the tissue (the use of isosulfan blue in the same setting required surgery to lift back the surrounding tissue). In further studies, SLNs were identified and effectively removed by QD-guided

Table 3. Nanomaterials used in cancer therapy. For each application, we provide details of the strategy adopted to deliver the nanomaterials to the tumor in in vivo experiments, as well as the physical properties of the nanomaterials on which the technique is based.

Application	Nanomaterial	In vitro	In vivo	Delivery	Physical property	Reference
Paclitaxel drug delivery	Gold NPs			–	Size, surface area	[125]
Methotrexate drug delivery	Magnetic NPs	√		Active targeting (methotrexate)	Size, surface area	[124]
Drug delivery and monitoring of release	QDs	√		Active targeting (A10 RNA aptamer)	FRET	[70]
Dispersion of hydrophobic drugs in water	Gold NPs	√		–	Size	[127,138]
Dispersion of hydrophobic drugs in water	Magnetic/silica core/shell NPs	√		–	–	[139]
Magnetically guided drug and gene delivery	Magnetic NPs	√	√	Magnetically guided	Magnetism	[126,131]
Magnetically guided drug and gene delivery	Liposome-embedded magnetic NPs		√	Intravenous injection + magnetic guidance	Size, magnetism	[132,133]
Magnetically guided drug and gene delivery	Liposome-embedded magnetic NPs		√	Intravenous injection + magnetic guidance + active targeting (anti-EGFR)	Size, magnetism	[135]
Magnetically guided drug and gene delivery	Ni-embedded carbon nanotubes	√		Magnetic guidance	Magnetism High surface area nanotube shape	[136]
Localized triggered drug release	Magnetic NPs			–	Néel relaxation	[128,129,141]
Localized triggered drug release	Gold NPs	√		–	Size	[145]
Localized triggered drug release	Gold nanoshells			–	Photothermal energy conversion	[143,144]
Localized triggered drug release	Gold nanorods	√		–	Photothermal energy conversion	[146]
Triggered release of multiple drugs	Gold nanorods			–	Photothermal energy conversion	[130]
Photodynamic therapy	QDs	√		–	Formation of toxic radicals under irradiation	[175,176]
Photodynamic therapy	Fullerenes	√	√	EPR	Formation of toxic radicals under irradiation	[170–174]
Radiation therapy	Gold NPs	√	√	EPR	High atomic number	[161,163–165]
Tumor cell thermal ablation	Gold NPs	√	√	Local injection	Radiofrequency generated heat	[191]
Tumor cell thermal ablation	Gold NPs	√		–	Photothermal energy conversion when aggregated	[154]
Tumor cell thermal ablation	Gold nanoshells	√	√	EPR Active targeting (anti-HER2)	Photothermal energy conversion	[110,151,155–159]
Tumor cell thermal ablation	Gold nanoshells	√		Nanoshell-loaded monocytes	Photothermal energy conversion	[160]
Tumor cell thermal ablation	Gold nanorods	√		Active targeting (anti-EGFR)	Photothermal energy conversion	[152]
Tumor cell thermal ablation	Hollow gold nanosphere	√	√	Injection Active targeting (anti-EGFR)	Photothermal energy conversion	[153]
Tumor cell thermal ablation	Magnetic NPs		√	Local injection	Néel relaxation	[149,150,192–196]

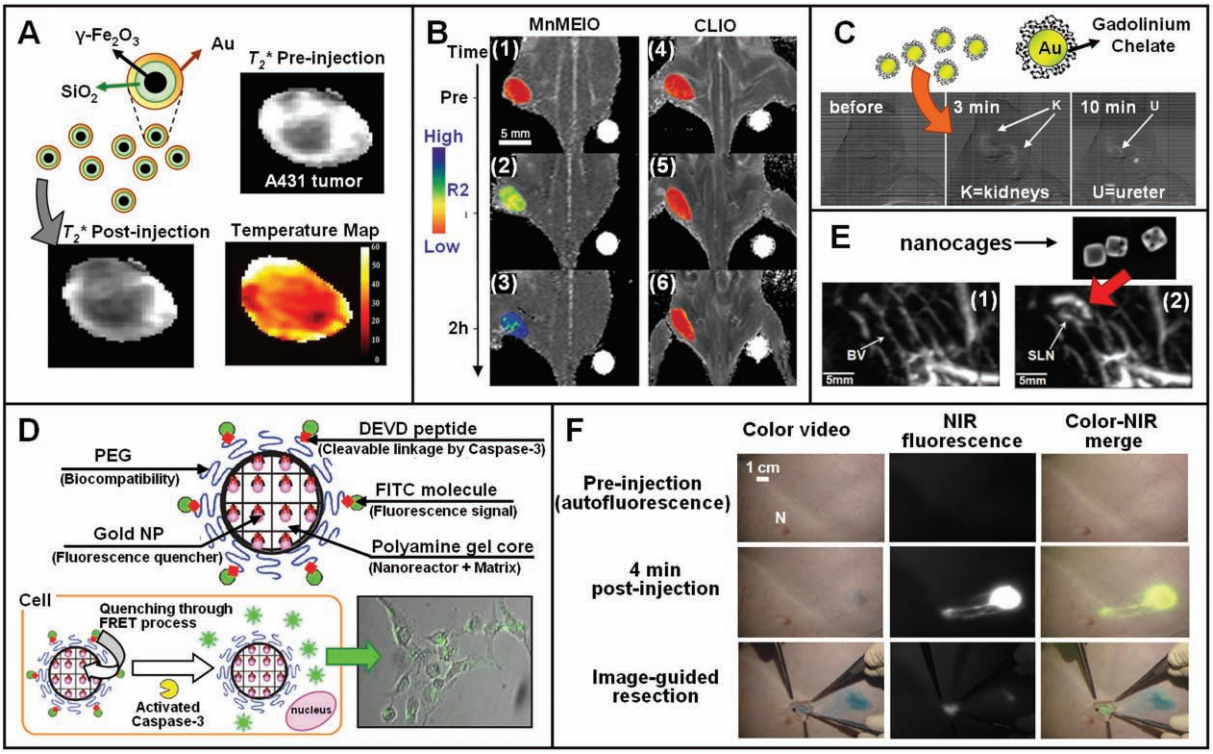

Figure 7. NPs as imaging contrast agents. A) T_2 MRI and the magnetic resonance temperature map of a subcutaneous A431 tumor injected with multifunctional magnetic/gold/silica NPs at a dose of 1×10^{11} particles/site. The darkening of the tumor in T_2-weighted MRI after the injection of the NPs and the increase in temperature by as much as 60 °C indicate the potential use of the NPs for simultaneous MRI and photothermal therapy. Adapted with permission.[110] Copyright 2009, Materials Research Society. B) In vivo MRI detection of cancer using engineered magnetic NP–Herceptin conjugates. 1–6) Color maps of T_2-weighted MRI images of a mouse implanted with the cancer cell line NIH3T6.7, at different time points after injection of magnetism-engineered iron oxide (MnMEIO)–Herceptin conjugates (1–3) or cross-linked iron oxide (CLIO)-Herceptin conjugates (4–6): pre-injection (1,4), and 1 h (2,5) or 2 h (3,6) after injection. In panels 1–3, gradual color changes at the tumor site, from red to blue, indicate progressive targeting by MnMEIO–Herceptin conjugates. In contrast, almost no change was seen in the mouse treated with CLIO–Herceptin conjugate (4,5,6). Adapted with permission.[111] Copyright 2007, Macmillan Publishers Ltd. C) Transmission mode planar X-ray images of a rat before and after injection of Gd chelate-coated gold NPs. The contrast of both the kidneys (K) and the ureter (U) is enhanced due to the introduction of the NP conjugates. Reproduced with permission.[117] Copyright 2008, American Chemical Society. D) Fluorescence quenching-based apoptosis nanoprobe. Cartoon: PEGylated *poly*diethylaminoethylmethacrylate (PEAMA) gel containing gold NPs within the cross-linked polymer core. FITC molecules are linked to the PEG chains via the NEVN peptide sequence. This sequence is specifically recognized and cleaved by protease caspase-3, which is active during apoptosis. The fluorescence of the FITC molecules linked to the gel is quenched by the gold NPs. In the presence of proteases the peptide linker is cleaved and the FITC molecules disperse into solution exhibiting fluorescence. Image: Confocal fluorescence image of HuH-7 cells incubated with the composite nanogel after induction of apoptosis by staurosporine. Adapted with permission.[118] E) In vivo noninvasive photoacoustic images of SLN in a rat acquired 1) before and 2) 194 min after intradermal injection of 0.2 pmol of 50 nm gold nanocages similar to those shown in the SEM image on the top. Reproduced with permission.[119] Copyright 2009, American Chemical Society. F) Images of the surgical field of a pig injected intradermally with 400 pmol of NIR-emitting QDs in the right groin for SLN mapping. Color video (left), NIR fluorescence (middle), and color-NIR merge (right, NIR fluorescence image pseudocolored in lime green) images are shown. The position of a nipple (N) is indicated. Adapted with permission.[120] Copyright 2004, Macmillan Publishers Ltd.

surgery in large animals such as pigs (Figure 7F). Their group intend to take this technology to clinical trial.[123]

3.2. NP-Assisted Cancer Therapies

Chemotherapy and radiotherapy are two of the most well-established cancer treatments available today. However, these treatments are nonetheless associated with negative side effects which can significantly affect the quality of life of patients. For example, numerous chemotherapeutic drugs target rapidly dividing cells and are delivered to the tumor site via the bloodstream. As a consequence, these drugs also end up damaging healthy cells, hence the spectrum of side effects. Radiotherapy utilizes ionizing radiation to damage the DNA of cancer cells or create toxic radicals in the presence of water molecules and oxygen, leading to cell death or a reduction in the cell replication rate. However, radiotherapy lacks specificity for tumoral tissue. Confining the therapy and therapeutic activity exclusively to the tumor site is therefore one of the big challenges for new technologies. EPR effect can facilitate the delivery and localization of NPs inside tumors. Drug circulation time and cancer specificity can be further enhanced by PEGylation of the NP surface and active targeting respectively. Different approaches to drug delivery involve the embedding of the NPs within organic particles that serve as delivery vectors for the drugs. In general, the drug release is achieved through enzymatic

or chemical degradation of the therapeutic molecule-NP linkers, charge interactions or degradation of the polymer matrix. The rational functionalization of NP surfaces with anticancer drugs and active targeting moieties also allows internalization of the drugs into the cells via precise pathways (e.g., **Figure 8**A).[124] It has been shown that even organic molecules with exceedingly complex structures such as the chemotherapeutic drug Paclitaxel can be covalently attached to gold NPs with high loading density and in a controlled fashion.[125] CytImmune Sciences Inc. has developed a series of drug-loaded gold NPs functionalized with PEG and tumor necrosis factor alpha (TNF-α) for active targeting. One of these therapeutics, Aurimune, is currently in Phase I human clinical trials.

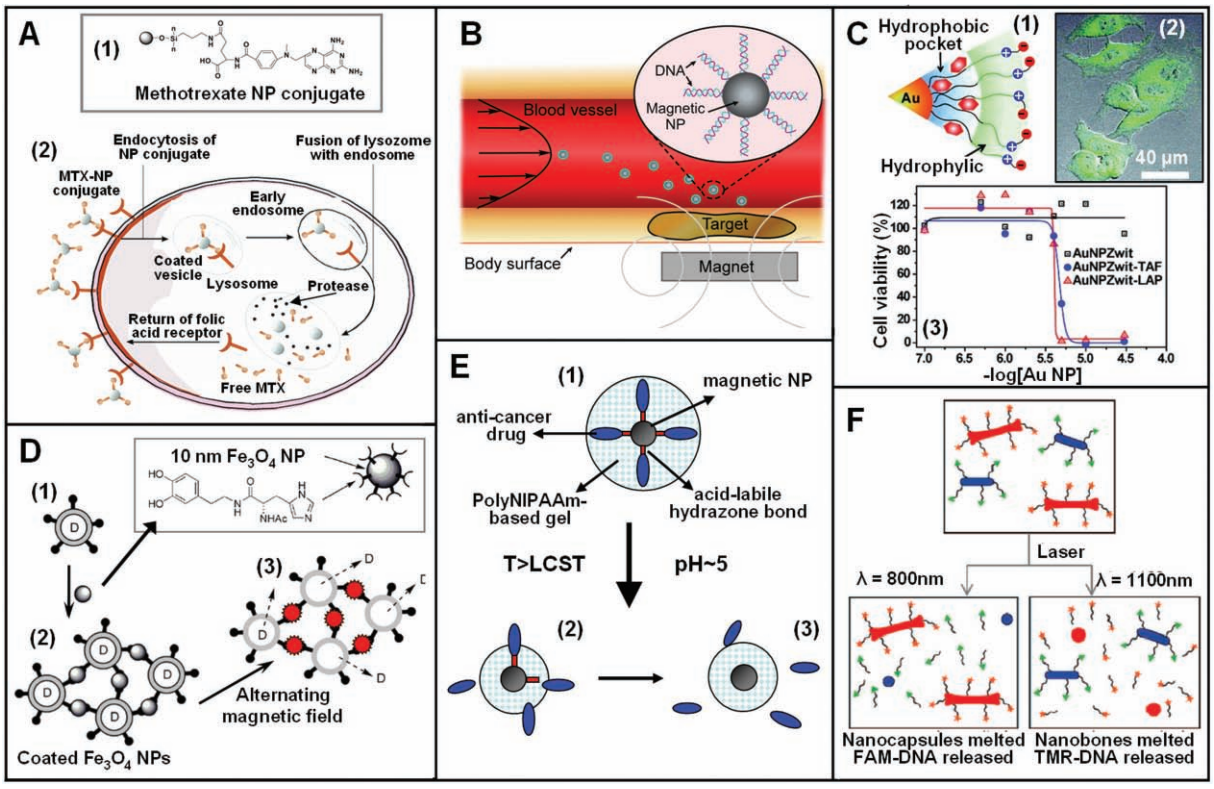

Figure 8. NP-based strategies for drug delivery. A) Example of magnetic NP-based system for combined drug delivery and MRI imaging. 1) Schematic of an iron oxide NP covalently bound with methotrexate (MTX), a chemotherapeutic drug that can target many types of cancer cell whose surfaces over-express folate receptors. 2) Proposed intracellular trafficking model of the uptake of MTX-modified NPs into cancer cells. Following their uptake via receptor-mediated endocytosis, NPs are transported to early endosomes. The endosomes then fuse with low pH lysosomes containing proteases, which cleave the peptide bond between the MTX and the NP, allowing the MTX to be released from the NP surface inside the target cell. Adapted with permission.[124] Copyright 2005, American Chemical Society. B) Schematic representation (side view section) of in vivo delivery of therapeutic magnetic NPs. Dashed gray rings indicate the lines of magnetic flux due to the ex vivo permanent magnet. The positioning of the magnet above the target will draw the magnetic NPs out of the bloodstream and towards the affected area. Readapted with permission.[126] C) 1) Gold NPs protected with ligands forming a hydrophobic pocket surrounding the NP. A hydrophilic shell composed of a tetra(ethylene glycol) unit terminated with a zwitterionic headgroup imparts solubility. The red hexagons represent fluorescent dye Bodipy, or anticancer drugs tamoxifen (TAF) and β-lapachone (LAP), which are trapped in the hydrophobic pocket. 2) Overlap of confocal fluorescence and bright field images of MCF-7 cell treated with Bodipy-conjugated NPs for 2 h. Transmission electron microscopy images (not shown) indicated that the fluorescent dye was delivered to the cells without uptake of NPs. 3) The NPs are not cytotoxic, but the NP-drug complexes are, as measured by Alamar blue assay after 24 h incubation with MCF-7 cells. Adapted with permission.[127] Copyright 2009, American Chemical Society. D) Formation of magnetic NP–vesicle assemblies, and potential use as magnetically triggered drug delivery vehicles. 1) Histidine–dopamine conjugate-coated magnetic NP and lipid vesicles containing fluorinated Cu-iminodiacetate (Cu(IDA))-capped lipids are mixed 2) to form NP-vesicles aggregates via histidine–Cu(IDA) interaction. 3) Upon application of an alternating magnetic field, the NPs increase their temperature triggering the melting of the lipid membrane and the consequent release of encapsulated drug. Adapted with permission.[128] Copyright 2009, Springer Science+Business Media. E) Schematic of a proposed core–shell drug delivery system for triggered release. 1) Anticancer drug doxorubicin is linked to magnetic NPs through an acid-labile hydrazone bond. The NPs are incorporated in a composite hydrogel made of PolyNIPAAm and enzymatically biodegradable dextran. For temperatures above the gel lower critical solution temperature (LCST ≅ 38°C) and mild acidic pH the anticancer drug is released through two distinct mechanisms: firstly, the rapid collapse of the thermosensitive polymer (2) and then the slower cleavage of the acid-labile linker (3). Adapted with permission.[129] Copyright 2007, Elsevier. F) Example of selective release by means of gold nanorods. Bottom-left: DNA-conjugated nanocapsules (blue ovals) and nanobones (red bones) are exposed to 800 nm irradiation, which is the nanocapsule SPR frequency. The radiation melts the nanocapsules and selectively releases the conjugated 6-carboxyfluorescein (FAM)-DNA (green triangles). Bottom-right: exposure to 1100 nm irradiation (nanobone SPR frequency) melts the nanobones, selectively releasing the conjugated tetramethylrhodamine (TMR)-DNA (orange stars). Adapted with permission.[130] Copyright 2009, American Chemical Society.

small NANO MICRO

Drug and gene uptake into cancer cells can be improved by using magnetic NPs, which can be effectively guided into tumors by means of external magnetic fields.[126] This approach has been applied to surface-functionalized NPs[126,131] (Figure 8B), NP-loaded liposomes[132,133] (so-called magnetoliposomes)[134] and highly effective oleic acid-coated magnetite nanocrystal cores with cationic lipid shells.[135] DNA-functionalized carbon nanotubes embedded with magnetic nickel NPs have also been used with nearly 100% transfection rates in lymphoma cells in vitro.[136] Due to their elongated shape, the nanotubes align with the direction of the magnetic flux and are moved like spears toward the cell membrane. This specific orientation aids the penetration of the particle-gene complex through the cell membrane and into the cytoplasm. A major drawback of magnetic NP-mediated delivery systems is the rapid decay in delivery efficiency within just a few centimeters of the magnetic source, due to the high field gradients required to guide the NPs.[137] Hence, the use of magnetic NPs for guided delivery may be limited in clinical practice because of the large size of humans and the position of internal organs deep within the body cavity.

Systems allowing not only drug delivery, but also the detection and monitoring of intracellular drug release combined with cell imaging have also been developed (Figure 4C).[70] The use of QDs in these systems opens up the possibility of multiplexed monitoring of the temporal release of multiple drugs, although toxicological issues related to the in vivo use of QDs need to be carefully addressed.

3.2.1. NP-Assisted Dispersion of Hydrophobic Drugs in Physiological Media

Certain drugs are hydrophobic in nature and thus have poor solubility in blood, and hence it is difficult to deliver them to tumors via the bloodstream. For example, photosensitizers used in photodynamic therapy are hydrophobic and tend to aggregate in aqueous media, leading to quenching and a lack of tissue selectivity. The suspension of photosensitizer molecules in water has been achieved by coating them onto metallic NPs,[138] which has the added effect of enhancing their photophysical properties. Alternatively, photosensitizers have been loaded into silica NPs via microemulsion and sol-gel methods.[139]

Gold NPs protected by a monolayer of amphiphilic thiols can provide an alternate strategy to tackle drug solubility problems. Hydrophobic pockets surrounding a gold NP are created via surface conjugation of thiol-terminated molecules containing both hydrophobic and hydrophilic moieties. The hydrophilic groups at the solvent interface impart water solubility to the particles. The hydrophobic groups located at the gold NP surface form a closed region with an associated volume. Organic solutes can be incorporated in the hydrophobic pocket,[140] allowing for the storage and delivery of active molecules. Using NPs engineered in this way, Kim and co-workers[127] succeeded in delivering the highly hydrophobic anticancer drugs tamoxifen and β-lapachone into human breast cancer cells in vitro (Figure 8C).

3.2.2. NP-Mediated Triggered Drug Release

Triggered drug release allows localization of drug activity to diseased areas alone. One of the strategies developed for this purpose is to use materials that are responsive to environmental stimuli such as temperature. For example, magnetic NPs subjected to an alternating magnetic field act as nanosized thermal generators causing the disruption of proximal lipid bilayers by melting. This phenomenon was exploited to trigger the release of drugs contained in lipid vesicles alongside the NPs.[141] The same effect has been observed in assemblies of magnetic NPs and drug-containing lipid vesicles, where NPs acted as crosslinkers between the individual vesicles to form large assemblies (Figure 8D).[128]

Poly(*N*-isopropylacrylamide) (PolyNIPAAm) is a well established thermoresponsive polymer that undergoes a transition from hydrophobic to hydrophilic when heated above its lower critical solution temperature. Hydrogels that shrink when the temperature is raised above 37 °C have been produced by conjugating PolyNIPAAm with molecules such as acrylamides.[142] This property makes PolyNIPAAm composites suitable candidates for use in triggered drug delivery, for example by incorporating magnetic NPs[129] (Figure 8E) and gold nanoshells[143,144] into PolyNIPAAm-based hydrogels.

Triggered drug release has also been achieved by conjugating drug molecules to the NP surface with photocleavable linkers.[145] Alternatively, irradiation of the NPs at their SPR frequency can induce nanorod melting and consequent release of bound therapeutics (Figure 8F).[130,146]

3.2.3. NP-Based Delivery and Release of Multiple Drugs

The efficacy of chemotherapy can be improved by the synergistic combination of multiple drugs with complementary properties. One issue concerning the use of anti-angiogenic agents inside tumors is that their action inhibits blood vessel growth, preventing the delivery of additional anticancer drugs. The incorporation of both therapeutics and anti-angiogenic agents in a combined system would help address this limitation. In fact, the anti-angiogenic agent might improve therapeutic efficacy by entrapping the anticancer drug inside the tumor after release. Hence, delivery systems that allow not only multiple drug loading but also controllable sequential drug release are desirable. Different strategies have been developed to incorporate more than one drug type into a single delivery system, but differences in drug loading efficiency, pharmacokinetics and administration timing make the engineering of such systems extremely challenging.[147] Wijaya and co-workers[130] proposed an elegant solution to the delivery and triggered release of multiple drugs by exploiting the unique optical properties of gold nanorods (Figure 8F). The SPR wavelength of gold nanorods can be tuned by changing their aspect ratio so that different populations of nanorods can be excited independently. Using this concept, two different DNA oligonucleotides were selectively released.

3.2.4. Inducing Hyperthermia Using NPs

Hyperthermia alters the function of many structural and enzymatic proteins within cells, which in turn affect cell

growth and differentiation and can induce apoptosis. Heat sources currently used for hyperthermia therapy[148] result in poor temperature homogeneity and effectiveness. These problems have been overcome by using specifically engineered NPs as heat sources and delivering them through the blood stream or by local injection. Using these particles, high temperatures can be achieved locally, without affecting adjacent healthy tissue. Although the use of magnetic NPs for tumor hyperthermia was first reported thirty years ago,[149] it took until 2003 for magnetic NP-based hyperthermia therapy to enter clinical trials (at Charité–University Medicine Berlin). In the trials, superparamagnetic iron oxide/aminosilane-type core/shell NPs were injected into the tumor area and subjected to a 100 kHz oscillating magnetic field. Under the action of the magnetic field, the coated NPs spread in the tumoral tissue (thermal bystander effect), improving cellular uptake and avoiding rapid removal by macrophages.[150] This phenomenon allows a single injection of NPs to be sufficient for ten consecutive treatment sessions, minimizing the invasiveness of the therapy.

Gold nanoshells,[151] nanorods[152] and hollow gold nanospheres (**Figure 9**A)[153] with SPR frequencies in the NIR range promise to be particularly suitable for cancer ablation therapy applications due to NIR being the optimal range for transmission through tissue with minimal damage. Additionally, while isolated NPs do not absorb NIR radiation, NP aggregates exhibit an SPR peak in the NIR and can also be used as heat sources for hyperthermia applications. Nam and co-workers[154] engineered 10 nm gold NPs which aggregate via electrostatic attraction only at the typical tumor intercellular pH. While dispersed NPs do not absorb NIR radiation, NP aggregates exhibit a SPR peak in the NIR and can be used as heat sources for hyperthermia applications. Cancer therapy utilizing silica/gold core/shell NPs from Nanospectra Bioscience, Inc. is currently in Phase I human clinical trials. In contrast with magnetic NPs, these nanoshells are generally directed into tumors through the vascular system, although they also accumulate nonspecifically in the spleen and liver.[155] In a further development, nanoshells have been functionalized to improve their specificity for tumor cells[156,157] and engineered to combine the therapeutic action with magnetic and fluorescent optical imaging for MRI (Figure 7A)[110,158,159] and intraoperative imaging (Figure 9B).[159] A "Trojan Horse" strategy to deliver nanoshells to hypoxic regions of solid tumors has also been developed making use of nanoshell-loaded monocytes. In fact, these cells are capable of entering the tumor due to chemoattractive gradients generated by hypoxia and necrotic conditions.[160]

3.2.5. NP-Enhanced Radiotherapy

Although widely used, radiotherapy has toxic effects on the tissue surrounding the tumor and also on internal organs. These side effects limit the amount of radiation that can be used during treatment. Radiation dose enhancement localized at the tumor area would enable lower doses of radiations and therefore reduced side effects. Radiation dose enhancement at the interface between high and low atomic

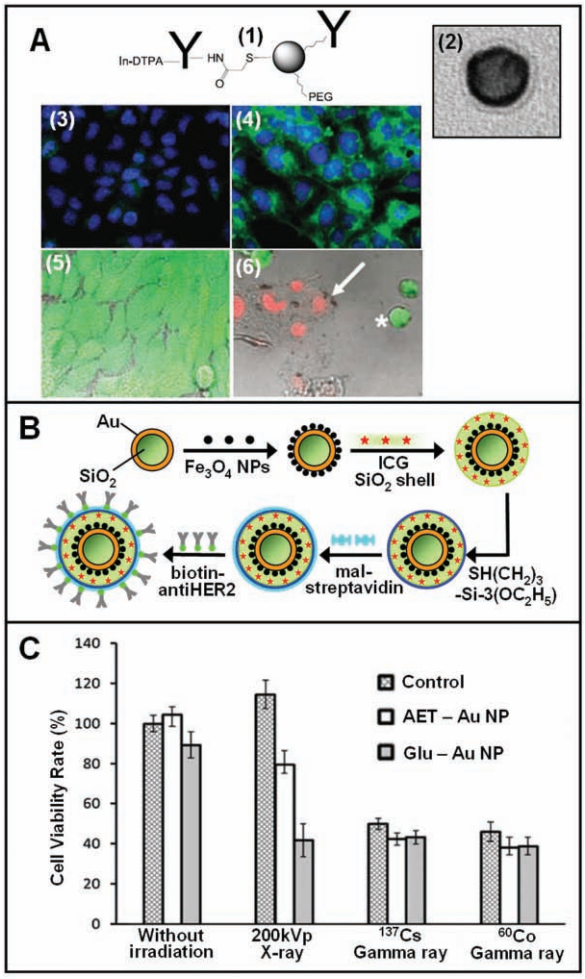

Figure 9. NP-based cancer therapy strategies. A) 1) Schematic and 2) Transmission electron microscopy image of anti-epidermal growth factor receptor (EGFR) monoclonal antibodies conjugated to hollow gold nanospheres (HAuNS, average diameter 30 nm). The antibodies are labeled with radiometal indium chelator (In-DTPI). 3,4) The overlay of fluorescence and light microscopy images (40× magnification) of human squamous carcinoma A431 cells incubated with HAuNS conjugated with mouse IgG and anti-EGFR respectively. Cells were stained for visualization of cell nuclei (blue). Light-scattering images of HAuNSs were pseudocolored green. Anti-EGFR-conjugated HAuNS selectively bind A431 cells. 5,6) The overlay of fluorescence microscopy images (400× magnification) of untreated cells and cells treated with anti-EGFR-conjugated-HAuNS and NIR laser respectively. Cells were stained for visualization of live cells (green) and dead cells (red). In (5) cells retained normal morphology with no apparent death observed. In contrast, in (6) the dead cells showed rounded morphology (asterisk) and membrane damage. Adapted with permission.[153] Copyright 2008, American Association for Cancer Research. B) Schematic diagram illustrating the fabrication of multifunctional NPs for MRI, intraoperative imaging and cancer ablation therapy. SiO_2/Au core/shell NPs are coated with magnetic NPs and silica doped with NIR fluorescent Indocyanine Green (ICG). Streptavidin-maleamides are covalently linked to the NP surface through thiolated silanes and bind biotinylated antibodies against HER2 for active targeting. Readapted with permission.[159] C) Radiation enhancement by means of gold NPs. Comparison of the cytotoxicity induced in breast cancer cell line by various types of irradiation in the presence of gold NPs functionalized with cysteamine (AET-GNPs) and thioglucose (Glu-GNPs) for active targeting (48 h after irradiation). Glu-GNPs significantly increased the cytotoxicity of 200 kVp X-rays, meaning lower doses of radiation can be used in the presence of NPs, reducing the risk of side effects. Reproduced with permission.[161]

NANO MICRO small

number materials for cancer therapy has been studied for more than 30 years.[162] However, in order to translate this finding into clinical benefit, readily available, easily utilized and nontoxic materials are required. In 2004, the suitability of gold NPs for radiotherapy was tested in vivo.[163] These NPs were described to localize into the tumor site via the EPR effect and there they were exposed to X-ray radiation. Mice injected with NPs demonstrated remarkable tumor regression in mammary tumors and long-term survival without any significant toxicity, thus indicating the utility of these nanomaterials for radiotherapy. Following this work, numerous experimental[161,164,165] and Monte Carlo simulation studies[166–168] have further elucidated the properties of NPs as radiation enhancers (Figure 9C).[161]

3.2.6. Nano-tools for Photodynamic Therapy

Photosensitizers are a particular class of anticancer drugs that become active and therefore cytotoxic only when excited at precise frequencies in the presence of molecular oxygen. Interestingly, as photosensitizers are fluorescent molecules, they also offer a means for tumor imaging. The use of fullerenes[169–174] and QDs[175] as photosensitizers has been attempted due to their capacity to generate reactive oxygen species when irradiated with light. QDs have also been used to effectively potentiate conventional photosensitizers.[176] However, issues related to fullerene insolubility in water and QD toxicity in the body have hindered their further development as therapeutics, although both types of NPs currently remain the focus of intense research.

4. Toxicological Considerations

Nanomaterials exhibit physical properties that are not observed in their bulk form. For this reason, toxicity can potentially be altered or enhanced in certain materials when they are confined at the nanoscale. The lack of a coherent body of knowledge on the subject, compounded by the sheer number of different types of NPs in use today, makes the prediction of novel nanomaterial toxicity challenging.[177] This issue has mainly hindered the use of NPs in in vivo applications, where the main sources of concern involve:[178,179] 1) the ability of NPs to enter the body and cells via multiple different mechanisms; 2) the small size of NPs permitting their interaction with subcellular structures such as proteins and DNA; 3) the large surface area of metal NPs acting as highly effective electron acceptors/donors and therefore able to generate damaging free radical species. Additionally, there are stability issues associated with NPs, such as their tendency to aggregate under certain conditions, meaning they can potentially expose individuals to risks of blood clotting, embolism and thrombosis. Other potential sources of toxicity include: the release of certain NP surface ligands, such as the surfactant currently used in nanorod synthesis; and the exposure of toxic elements such as Cd (contained within some QDs) resulting from surface oxidation, which is strongly enhanced by exposure of the QDs to high energy radiation such as UV light.[180] While gold NPs have shown relatively high levels of cellular uptake without causing acute cytotoxicity,[181] the toxicity of QDs was found to depend on their inherent physicochemical properties and environmental conditions.[182] Concerns on QD toxicity have triggered the development of Cd-free QDs,[183] stable photoluminescent silicon QDs in water[184] and a number of alternative high-luminescent systems such as, for example, organic dye-silica core–shell NPs (**Figure 10**),[185,186] and aptamer-conjugated silica NPs for FRET-based multiplexed imaging of multiple cancer cell lines.[187] Liposome fusion onto mesoporous silica particles has also been used to simultaneously load and seal the cargo, creating a system useful for imaging, delivery across the cell membrane and controlled release.[188]

Nanomaterials have been recognized as a growing source of technological innovation by governmental, academic and industrial parties. Through recognition of the risks as well as the potential benefits of this new technology, numerous consortiums have been set up worldwide to establish regulatory frameworks. In Europe, for example, the European Community has funded an interdisciplinary portfolio of research projects aiming to elucidate the health and environmental implications of nanomaterials and to provide recommendations for the safe handling of such materials.[189] Importantly, in February 2009, the European Food Safety Authority (EFSA) adopted the recommendations of its scientific committee[190] namely that nanomaterials should be treated as distinct materials, and that each new application of nanomaterials should be separately investigated.

5. Future Perspectives and Conclusion

Newly-developed nanomaterials offer unique opportunities in cancer treatment as a complement to current medical

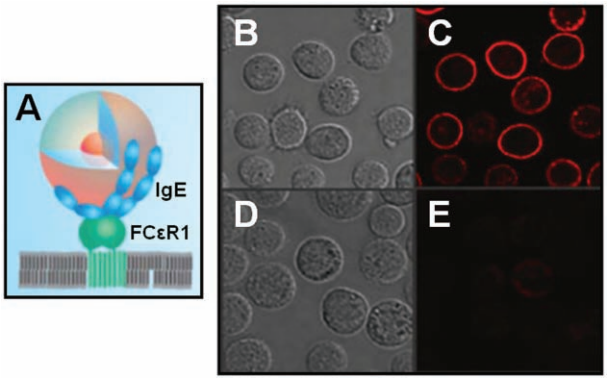

Figure 10. Rat Basophilic Leukemia (RBL) cell labeling using fluorescent organic dye-silica core–shell NPs with IgE antibody adsorbed on their surface. Here, the silica shell enhances the dye optical properties and confers biocompatibility, as well as a uniform, well-known chemistry, at the expense of complex and dye-specific synthesis protocols. The NPs specifically attach to the surface receptor of a cell via the IgE–FcεRI interaction as schematically depicted in (A). Bright field (B) and confocal fluorescence (C) images of RBL cells with IgE-mediated cell surface labeling. As a control, bright field (D) and fluorescence (E) images of RBL cells incubated with free IgE antibodies to quench the FcεRI receptors before incubation with the NP–IgE complexes, showing minimal nonspecific cell surface binding. Adapted with permission.[185] Copyright 2007, PCCP Owner Societies.

technology. Due to their novel properties and multifunctional capabilities, NPs provide new strategies for a range of applications, from improved cancer diagnosis and imaging to targeted therapy.

While the use of NPs for biosensor development is in many cases ready for commercial translation, the in vivo clinical applications of NPs are subject to the complete assessment of their potential toxicity. Promisingly, the first NP-based cancer diagnostic tool has been commercialized and some NP-based cancer therapeutics are currently in human clinical trials.

The ultimate challenge for cancer treatment is to be able to diagnose and cure cancer without surgical intervention and avoiding the occurrence of side effects. New technology should aim therefore to discover new cancer markers and develop highly reliable and sensitive screening tests, as well as effective localized therapies. Current nanotechnology-based sensing systems may provide advantages in monitoring the recurrence of a disease. NP multiplexing capability promises to make a diagnosis more accurate through the detection of a cocktail of biomarkers related to a specific condition. Drug delivery through active and passive targeting strategies has proved successful in localizing therapeutic activity of anticancer drugs at the tumor site. From a therapeutic point of view this achievement means that higher drug payload can be used with minimized side effects. However, strategies relying on delivery via the blood stream can only be used after the tumor has developed its own vasculature. More sophisticated strategies will be required for the early detection, imaging, and delivery of drugs into pre-angiogenic tumors for early-stage cancer treatment.

Acknowledgements

CM was funded by the European Community's Seventh Framework Programme under grant agreement PIEF-GA-2008–219573. SBL was funded by an EPSRC DTA grant. MMS thanks the EPSRC "Challenging Engineering" and the ERC "Naturale" grants.

[1] World Health Organization, 2008–2013 *Action Plan for the Global Strategy for the Prevention and Control of Noncommunicable Diseases 2008*, http://www.who.int/nmh/publications/9789241597418/en/index.html (accessed August, 2010).
[2] L. M. Meyer, F. R. Miller, M. J. Rowen, G. B. Julius Rutzky, *Acta Haematol.* **1950**, *4*, 157–167.
[3] G. Gregoriadis, C. P. Swain, E. J. Wills, A. S. Tavill, *Lancet* **1974**, *303*, 1313–1316
[4] M. F. G. Stevens, J. A. Hickman, S. P. Langdon, D. Chubb, L. Vickers, R. Stone, G. Baig, C. Goddard, N. W. Gibson, J. A. Slack, C. Newton, E. Lunt, C. Fizames, F. Lavelle, *Cancer Res* **1987**, *47*, 5846–5852.
[5] D. S. Shane, *Cancer Practice* **1998**, *6*, 195–197.
[6] C. A. Hudis, *N. Engl. J. Med.* **2007**, *357*, 39–51.
[7] D. Luo, W. M. Saltzman, *Nat. Biotechnol.* **2000**, *18*, 33–37.
[8] M. Ferrari, *Nat. Rev. Cancer* **2005**, *5*, 161–171.
[9] M. E. Davis, Z. Chen, D. M. Shin, *Nat. Rev. Drug Discov.* **2008**, *7*, 771–782.
[10] R. Duncan, *Nat. Rev. Cancer* **2006**, *6*, 688–701.
[11] M. E. Gindy, R. K. Prud'homme, *Expert Opin. Drug Deliv.* **2009**, *6*, 865–878.
[12] M. J. Bissell, D. Radisky, *Nat. Rev. Cancer* **2001**, *1*, 46–54.
[13] A. Jones, A. L. Harris, *Cancer J. Sci. Am.* **1998**, *4*, 209–217.
[14] G. Bergers, L. E. Benjamin, *Nat. Rev. Cancer* **2003**, *3*, 401–410.
[15] Y. Matsumura, H. Maeda, *Cancer Res.* **1986**, *46*, 6387–6392.
[16] D. P. O'Neal, L. R. Hirsch, N. J. Halas, J. D. Payne, J. L. West, *Cancer Lett.* **2004**, *209*, 171–176.
[17] P. Vaupel, D. K. Kelleher, M. Hockel, *Semin. Oncol.* **2001**, *28*, 29–35.
[18] M. Stubbs, P. M. J. McSheehy, J. R. Griffiths, C. L. Bashford, *Mol. Med. Today* **2000**, *6*, 15–19.
[19] D. M. Prescott, H. C. Charles, J. M. Poulson, R. L. Page, D. E. Thrall, Z. Vujaskovic, M. W. Dewhirst, *Clinical Cancer Res.* **2000**, *6*, 2501–2505.
[20] E. S. Lee, Z. Gao, Y. H. Bae, *J. Control. Release* **2008**, *132*, 164–170.
[21] J. A. Ludwig, J. N. Weinstein, *Nat. Rev. Cancer* **2005**, *5*, 845–856.
[22] J. A. Ludwig, *Curr. Oncology Rep.* **2008**, *10*, 329–337.
[23] K. F. Pirollo, E. H. Chang, *Trends Biotechnol.* **2008**, *26*, 552–558.
[24] R. T. Allen, W. J. Hunter, D. K. Agrawal, *J. Pharmacol. Toxicol. Methods* **1997**, *37*, 215–228.
[25] D. K. Biswas, A. P. Cruz, E. Gansberger, A. B. Pardee, *Proc. Natl. Acad. Sci. USA* **2000**, *97*, 8542–8547.
[26] K. de Bruin, N. Ruthardt, K. von Gersdorff, R. Bausinger, E. Wagner, M. Ogris, C. Brauchle, *Mol. Ther.* **2007**, *15*, 1297–1305.
[27] G. L. Semenza, *Nat. Rev. Cancer* **2003**, *3*, 721–732.
[28] E. Ruoslahti, *Nat. Rev. Cancer* **2002**, *2*, 83–90.
[29] G. Mie, Leipzig, *Ann. Phys.* **1908**, *330*, 377–445.
[30] A. Gole, C. J. Murphy, *Chem. Mater.* **2004**, *16*, 3633–3640.
[31] R. D. Averitt, S. L. Westcott, N. J. Halas, *J. Opt. Soc. Am. B-Opt. Phys.* **1999**, *16*, 1824–1832.
[32] H. B. Na, I. C. Song, T. Hyeon, Adv. Mater. 2009, 21, 2133–2148.
[33] K. E. Sapsford, L. Berti, I. L. Medintz, *Angew. Chem. Int. Ed.* **2006**, *45*, 4562–4588.
[34] S. J. Oldenburg, J. B. Jackson, S. L. Westcott, N. J. Halas, Appl. Phys. Lett. 1999, 75, 2897–2899.
[35] A. O. Govorov, H. H. Richardson, *Nano Today* **2007**, *2*, 30–38.
[36] S. Mornet, S. Vasseur, F. Grasset, E. Duguet, *J. Mater. Chem.* **2004**, *14*, 2161–2175.
[37] C. Sun, J. S. H. Lee, M. Q. Zhang, *Adv. Drug Delivery Rev.* **2008**, *60*, 1252–1265.
[38] J. P. Fortin, F. Gazeau, C. Wilhelm, *Eur. Biophys. J. Biophys. Lett.* **2008**, *37*, 223–228.
[39] R. Hergt, W. Andra, C. G. d'Ambly, I. Hilger, W. A. Kaiser, U. Richter, H. G. Schmidt, *IEEE Trans. Magn.* **1998**, *34*, 3745–3754.
[40] R. E. Rosensweig, *J. Magn. Magn. Mater.* **2002**, *252*, 370–374.
[41] X. Michalet, F. F. Pinaud, L. A. Bentolila, J. M. Tsay, S. Doose, J. J. Li, G. Sundaresan, A. M. Wu, S. S. Gambhir, S. Weiss, *Science* **2005**, *307*, 538–544.
[42] M. Bruchez, M. Moronne, P. Gin, S. Weiss, A. P. Alivisatos, *Science* **1998**, *281*, 2010–2016.
[43] W. C. W. Chan, S. Nie, *Science* **1998**, *281*, 2016–2018.
[44] A. P. Alivisatos, *Science* **1996**, *271*, 933–937.
[45] X. Y. Wu, H. J. Liu, J. Q. Liu, K. N. Haley, J. A. Treadway, J. P. Larson, N. F. Ge, F. Peale, M. P. Bruchez, *Nat. Biotechnol.* **2003**, *21*, 41–46.
[46] E. R. Goldman, A. R. Clapp, G. P. Anderson, H. T. Uyeda, J. M. Mauro, I. L. Medintz, H. Mattoussi, *Anal. Chem.* **2003**, *76*, 684–688.
[47] J. R. E. Shepard, *Anal. Chem.* **2006**, *78*, 2478–2486.
[48] L. Niu, W. Knoll, *Anal. Chem.* **2007**, *79*, 2695–2702.

[49] M. Y. Han, X. H. Gao, J. Z. Su, S. Nie, *Nat. Biotechnol.* **2001**, *19*, 631–635.
[50] S. I. Stoeva, J.-S. Lee, J. E. Smith, S. T. Rosen, C. A. Mirkin, *J. Am. Chem. Soc.* **2006**, *128*, 8378–8379.
[51] S. Schlucker, B. Kustner, A. Punge, R. Bonfig, A. Marx, P. Strobel, *J. Raman Spectrosc.* **2006**, *37*, 719–721.
[52] T. Förster, *Annalen der Physik* **1948**, *437*, 55–75.
[53] M. K. Wagner, F. Li, J. Li, X. F. Li, X. C. Le, *Anal. Bioanal. Chem.* **2010**, *397*, 3213–3224.
[54] I. L. Medintz, A. R. Clapp, F. M. Brunel, T. Tiefenbrunn, H. Tetsuo Uyeda, E. L. Chang, J. R. Deschamps, P. E. Dawson, H. Mattoussi, *Nat. Mater.* **2006**, *5*, 581–589.
[55] I. L. Medintz, H. Mattoussi, *Phys. Chem. Chem. Phys.* **2009**, *11*, 17–45.
[56] A. R. Clapp, I. L. Medintz, J. M. Mauro, B. R. Fisher, M. G. Bawendi, H. Mattoussi, *J. Am. Chem. Soc.* **2003**, *126*, 301–310.
[57] Z. Xia, Y. Xing, M.-K. So, A. L. Koh, R. Sinclair, J. Rao, *Anal. Chem.* **2008**, *80*, 8649–8655.
[58] Y. P. Kim, Y. H. Oh, E. Oh, S. Ko, M. K. Han, H. S. Kim, *Anal. Chem.* **2008**, *80*, 4634–4641.
[59] Department of Health UK, *Cancer Reform Strategy – second annual report*, *2009,* http://www.dh.gov.uk/en/Publicationsandstatistics/Publications/PublicationsPolicyAndGuidance/DH_109338 (accessed August, 2010).
[60] World Health Organization, *National Cancer Control Programmes – Policies and managerial guidelines 2002*, http://www.who.int/cancer/nccp/nccp/en/(accessed August, 2010).
[61] H. Xu, M. Y. Sha, E. Y. Wong, J. Uphoff, Y. Xu, J. A. Treadway, A. Truong, E. O'Brien, S. Asquith, M. Stubbins, N. K. Spurr, E. H. Lai, W. Mahoney, *Nucl. Acids Res.* **2003**, *31*, e43.
[62] J.-M. Nam, C. S. Thaxton, C. A. Mirkin, *Science* **2003**, *301*, 1884–1886.
[63] S. I. Stoeva, J.-S. Lee, C. S. Thaxton, C. A. Mirkin, *Angew. Chem. Int. Ed.* **2006**, *45*, 3303–3306.
[64] D. S. Grubisha, R. J. Lipert, H. Y. Park, J. Driskell, M. D. Porter, *Anal. Chem.* **2003**, *75*, 5936–5943.
[65] V. Mani, B. V. Chikkaveeraiah, V. Patel, J. S. Gutkind, J. F. Rusling, *ACS Nano* **2009**, *3*, 585–594.
[66] D. Gerion, F. Q. Chen, B. Kannan, A. H. Fu, W. J. Parak, D. J. Chen, A. Majumdar, A. P. Alivisatos, *Anal. Chem.* **2003**, *75*, 4766–4772.
[67] J. J. Storhoff, R. Elghanian, R. C. Mucic, C. A. Mirkin, R. L. Letsinger, *J. Am. Chem. Soc.* **1998**, *120*, 1959–1964.
[68] J. H. Li, X. Chu, Y. L. Liu, J. H. Jiang, Z. M. He, Z. W. Zhang, G. L. Shen, R. Q. Yu, *Nucl. Acids Res.* **2005**, *33*, E168.
[69] L. F. Shi, V. De Paoli, N. Rosenzweig, Z. Rosenzweig, *J. Am. Chem. Soc.* **2006**, *128*, 10378–10379.
[70] V. Bagalkot, L. Zhang, E. Levy-Nissenbaum, S. Jon, P. W. Kantoff, R. Langer, O. C. Farokhzad, *Nano Lett.* **2007**, *7*, 3065–3070.
[71] W. J. Catalona, J. P. Richie, F. R. Ahmann, M. A. Hudson, P. T. Scardino, R. C. Flanigan, J. B. DeKernion, T. L. Ratliff, L. R. Kavoussi, B. L. Dalkin, W. B. Waters, M. T. MacFarlane, P. C. Southwick, *J. Urol.* **1994**, *151*, 1283–1290.
[72] C. S. Thaxton, R. Elghanian, A. D. Thomas, S. I. Stoeva, J.-S. Lee, N. D. Smith, A. J. Schaeffer, H. Klocker, W. Horninger, G. Bartsch, C. A. Mirkin, *Proc. Natl. Acad. Sci. USA* **2009**, *106*, 18437–18442.
[73] A. Laromaine, L. L. Koh, M. Murugesan, R. V. Ulijn, M. M. Stevens, *J. Am. Chem. Soc.* **2007**, *129*, 4156–4157.
[74] E. D. Goluch, J. M. Nam, D. G. Georganopoulou, T. N. Chiesl, K. A. Shaikh, K. S. Ryu, A. E. Barron, C. A. Mirkin, C. Liu, *Lab Chip* **2006**, *6*, 1293–1299.
[75] X. Liu, Q. Dai, L. Austin, J. Coutts, G. Knowles, J. H. Zou, H. Chen, Q. Huo, *J. Am. Chem. Soc.* **2008**, *130*, 2780–2782.
[76] K. Kerman, T. Endo, M. Tsukamoto, M. Chikae, Y. Takamura, E. Tamiya, *Talanta* **2007**, *71*, 1494–1499.
[77] W. J. Catalona, A. W. Partin, K. M. Slawin, M. K. Brawer, R. C. Flanigan, A. Patel, J. P. Richie, J. B. deKernion, P. C. Walsh, P. T. Scardino, P. H. Lange, E. N. P. Subong, R. E. Parson, G. H. Gasior, K. G. Loveland, P. C. Southwick, *J. Am. Med. Ass.* **1998**, *279*, 1542–1547.
[78] D. Zheng, D. S. Seferos, D. A. Giljohann, P. C. Patel, C. A. Mirkin, *Nano Lett.* **2009**, *9*, 3258–3261.
[79] C.-C. Huang, S.-H. Chiu, Y.-F. Huang, H.-T. Chang, *Anal. Chem.* **2007**, *79*, 4798–4804.
[80] C. Xie, F. Xu, X. Huang, C. Dong, J. Ren, *J. Am. Chem. Soc.* **2009**, *131*, 12763–12770.
[81] G. T. Song, C. E. Chen, J. S. Ren, X. G. Qu, *ACS Nano* **2009**, *3*, 1183–1189.
[82] Z. X. Wang, R. Levy, D. G. Fernig, M. Brust, *J. Am. Chem. Soc.* **2006**, *128*, 2214–2215.
[83] J. E. Rundhaug, *Clin. Cancer Res.* **2003**, *9*, 551–554.
[84] R. C. Maher, S. A. Maier, L. F. Cohen, L. Koh, A. Laromaine, J. A. G. Dick, M. M. Stevens, *J. Phys. Chem. C* **2010**, *114*, 7231–7235.
[85] E. Chang, J. S. Miller, J. Sun, W. W. Yu, V. L. Colvin, R. Drezek, J. L. West, *Biochem. Biophys. Res. Commun.* **2005**, *334*, 1317–1321.
[86] I. L. Medintz, T. Pons, S. A. Trammell, A. F. Grimes, D. S. English, J. B. Blanco-Canosa, P. E. Dawson, H. Mattoussi, *J. Am. Chem. Soc.* **2008**, *130*, 16745–16756.
[87] A. Sancar, *Annu. Rev. Genet.* **1995**, *29*, 69–105.
[88] Z. Yu, J. Chen, B. N. Ford, M. E. Brackley, B. W. Glickman, *Environ. Mol. Mutagen.* **1999**, *33*, 3–20.
[89] H. Sugimura, T. Kohno, K. Wakai, K. Nagura, K. Genka, H. Igarashi, B. J. Morris, S. Baba, Y. Ohno, C. M. Gao, Z. Y. Li, J. D. Wang, T. Takezaki, K. Tajima, T. Varga, T. Sawaguchi, J. K. Lum, J. J. Martinson, S. Tsugane, T. Iwamasa, K. Shinmura, J. Yokota, *Cancer Epidemiol. Biomarkers Prev.* **1999**, *8*, 669–674.
[90] A. G. Kanaras, Z. X. Wang, M. Brust, R. Cosstick, A. D. Bates, *Small* **2007**, *3*, 590–594.
[91] X. Y. Xu, M. S. Han, C. A. Mirkin, *Angew. Chem. Int. Ed.* **2007**, *46*, 3468–3470.
[92] J. R. Glass, J. C. Dickerson, D. A. Schultz, *Anal. Biochem.* **2006**, *353*, 209–216.
[93] M. E. M. Noble, J. A. Endicott, L. N. Johnson, *Science* **2004**, *303*, 1800–1805.
[94] P. Cohen, *Nat. Rev. Drug Discov.* **2002**, *1*, 309–315.
[95] J. Oishi, Y. Asami, T. Mori, J. H. Kang, M. Tanabe, T. Niidome, Y. Katayama, *ChemBioChem* **2007**, *8*, 875–879.
[96] R. Freeman, T. Finder, R. Gill, I. Willner, *Nano Letters* **2010**, *10*, 2192–2196.
[97] J. E. Ghadiali, B. E. Cohen, M. M. Stevens, *ACS Nano* **2010**, *4*, 4915–4919.
[98] W. Lu, S. R. Arumugam, D. Senapati, A. K. Singh, T. Arbneshi, S. A. Khan, H. Yu, P. C. Ray, *ACS Nano* **2010**, *4*, 1739–1749.
[99] M. Chu, X. Song, D. Cheng, S. Liu, J. Zhu, *Nanotechnol.* **2006**, *17*, 3268–3273.
[100] Y. Xing, A. M. Smith, A. Agrawal, G. Ruan, S. Nie, *Int. J. Nanomed.* **2006**, *1*, 473–481.
[101] T. L. Andresen, S. S. Jensen, K. Jorgensen, *Prog. Lipid Res.* **2005**, *44*, 68–97.
[102] J. B. Wolinsky, M. W. Grinstaff, *Adv. Drug Delivery Rev.* **2008**, *60*, 1037–1055.
[103] P. Molyneux, *Water-Soluble Synthetic Polymers: Properties and Behavior*, Vol. 1–2, CRC Press, Florida, **1982**.
[104] J. M. Harris, R. B. Chess, *Nat. Rev. Drug Discov.* **2003**, *2*, 214–221.
[105] F. M. Veronese, G. Pasut, *Drug Discov. Today* **2005**, *10*, 1451–1458.
[106] E. B. Voura, *Nat. Med.* **2004**, *10*, 993–998.
[107] M. Stroh, *Nat. Med.* **2005**, *11*, 678–682.

[108] A. G. Filler, *Nat. Prec.* **2009**, doi:10.1038/npre.2009.3267.5.
[109] J. V. Frangioni, *J. Clin. Oncol.* **2008**, *26*, 4012–4021.
[110] M. P. Melancon, W. Lu, C. Li, *MRS Bull.* **2009**, *34*, 415–421.
[111] J. H. Lee, Y. M. Huh, Y. Jun, J. Seo, J. Jang, H. T. Song, S. Kim, E. J. Cho, H. G. Yoon, J. S. Suh, J. Cheon, *Nat. Med.* **2007**, *13*, 95–99.
[112] P. M. Winter, A. M. Morawski, S. D. Caruthers, R. W. Fuhrhop, H. Zhang, T. A. Williams, J. S. Allen, E. K. Lacy, J. D. Robertson, G. M. Lanza, S. A. Wickline, *Circulation* **2003**, *108*, 2270–2274.
[113] K. A. Hultborn, L. G. Larsson, I. Ragnhull, *Acta Radiol.* **1955**, *43*, 52–64.
[114] D. Kim, S. Park, J. H. Lee, Y. Y. Jeong, S. Jon, *J. Am. Chem. Soc.* **2007**, *129*, 7661–7665.
[115] C. S. Kim, P. Wilder-Smith, Y. C. Ahn, L. H. L. Liaw, Z. P. Chen, Y. J. Kwon, *J. Biomed. Opt.* **2009**, *14*, 034008.
[116] X. Qian, *Nat. Biotechnol.* **2008**, *26*, 83–90.
[117] C. Alric, J. Taleb, G. r. L. Duc, C. l. Mandon, C. Billotey, A. L. Meur-Herland, T. Brochard, F. Vocanson, M. Janier, P. Perriat, S. p. Roux, O. Tillement, *J. Am. Chem. Soc.* **2008**, *130*, 5908–5915.
[118] M. Oishi, A. Tamura, T. Nakamura, Y. Nagasaki, *Adv. Funct. Mater.* **2009**, *19*, 827–834.
[119] K. H. Song, C. H. Kim, C. M. Cobley, Y. N. Xia, L. V. Wang, *Nano Lett.* **2009**, *9*, 183–188.
[120] S. Kim, Y. T. Lim, E. G. Soltesz, A. M. De Grand, J. Lee, A. Nakayama, J. A. Parker, T. Mihaljevic, R. G. Laurence, D. M. Dor, L. H. Cohn, M. G. Bawendi, J. V. Frangioni, *Nat. Biotechnol.* **2004**, *22*, 93–97.
[121] J. V. Frangioni, S.-W. Kim, S. Ohnishi, S. Kim, M. G. Bawendi, *Methods Mol. Biol.* **2007**, *374*, 147–159.
[122] C. P. Parungo, Y. L. Colson, S. W. Kim, S. Kim, L. H. Cohn, M. G. Bawendi, J. V. Frangioni, *Chest* **2005**, *127*, 1799–1804.
[123] M. J. Liptay, *Ann. Thorac. Surg.* **2008**, *85*, S778–S779.
[124] N. Kohler, C. Sun, J. Wang, M. Zhang, *Langmuir* **2005**, *21*, 8858–8864.
[125] J. D. Gibson, B. P. Khanal, E. R. Zubarev, *J. Am. Chem. Soc.* **2007**, *129*, 11653–11661.
[126] J. Dobson, *Gene Ther.* **2006**, *13*, 283–287.
[127] C. K. Kim, P. Ghosh, C. Pagliuca, Z.-J. Zhu, S. Menichetti, V. M. Rotello, *J. Am. Chem. Soc.* **2009**, *131*, 1360–1361.
[128] R. J. Mart, K. P. Liem, S. J. Webb, *Pharm. Res.* **2009**, *26*, 1701–1710.
[129] J. Zhang, R. D. K. Misra, *Acta Biomater.* **2007**, *3*, 838–850.
[130] A. Wijaya, S. B. Schaffer, I. G. Pallares, K. Hamad-Schifferli, *ACS Nano* **2009**, *3*, 80–86.
[131] C. Mah, T. J. Fraites, I. Zolotukhin, S. H. Song, T. R. Flotte, J. Dobson, C. Batich, B. J. Byrne, *Mol. Ther.* **2002**, *6*, 106–112.
[132] T. Kubo, T. Sugita, S. Shimose, Y. Nitta, Y. Ikuta, T. Murakami, *Int. J. Oncol.* **2001**, *18*, 121–125.
[133] H. Nobuto, T. Sugita, T. Kubo, S. Shimose, Y. Yasunaga, T. Murakami, M. Ochi, *Int. J. Cancer* **2004**, *109*, 627–635.
[134] M. Cuyper, *Eur. Biophys. J.* **1988**, *15*, 311–319.
[135] Y. Namiki, T. Namiki, H. Yoshida, Y. Ishii, A. Tsubota, S. Koido, K. Nariai, M. Mitsunaga, S. Yanagisawa, H. Kashiwagi, Y. Mabashi, Y. Yumoto, S. Hoshina, K. Fujise, N. Tada, *Nat. Nanotechnol.* **2009**, *4*, 598–606.
[136] D. Cai, J. M. Mataraza, Z. H. Qin, Z. P. Huang, J. Y. Huang, T. C. Chiles, D. Carnahan, K. Kempa, Z. F. Ren, *Nat. Methods* **2005**, *2*, 449–454.
[137] A. D. Grief, G. Richardson, *J. Magn. Magn. Mater.* **2005**, *293*, 455–463.
[138] D. C. Hone, P. I. Walker, R. Evans-Gowing, S. FitzGerald, A. Beeby, I. Chambrier, M. J. Cook, D. A. Russell, *Langmuir* **2002**, *18*, 2985–2987.
[139] Z.-L. Chen, Y. Sun, P. Huang, X.-X. Yang, X.-P. Zhou, *Nanoscale Res. Lett.* **2009**, *4*, 400–408.
[140] M. Lucarini, P. Franchi, G. F. Pedulli, C. Gentilini, S. Polizzi, P. Pengo, P. Scrimin, L. Pasquato, *J. Am. Chem. Soc.* **2005**, *127*, 16384–16385.
[141] M. Babincová, P. Cicmanec, V. Altanerová, C. Altaner, P. Babinec, *Bioelectrochem.* **2002**, *55*, 17–19.
[142] C. S. Brazel, N. A. Peppas, *Macromolecules* **1995**, *28*, 8016–8020.
[143] M. Bikram, A. M. Gobin, R. E. Whitmire, J. L. West, *J. Controlled Release* **2007**, *123*, 219–227.
[144] S. R. Sershen, S. L. Westcott, N. J. Halas, J. L. West, *J. Biomed. Mater. Res.* **2000**, *51*, 293–298.
[145] S. S. Agasti, A. Chompoosor, C. C. You, P. Ghosh, C. K. Kim, V. M. Rotello, *J. Am. Chem. Soc.* **2009**, *131*, 5728–5729.
[146] C. C. Chen, Y. P. Lin, C. W. Wang, H. C. Tzeng, C. H. Wu, Y. C. Chen, C. P. Chen, L. C. Chen, Y. C. Wu, *J. Am. Chem. Soc.* **2006**, *128*, 3709–3715.
[147] S. Sengupta, D. Eavarone, I. Capila, G. L. Zhao, N. Watson, T. Kiziltepe, R. Sasisekharan, *Nature* **2005**, *436*, 568–572.
[148] J. Van Der Zee, *Ann. Oncology* **2002**, *13*, 1173–1184.
[149] R. T. Gordon, J. R. Hines, D. Gordon, *Med. Hypotheses* **1979**, *5*, 83–102.
[150] A. Jordan, R. Scholz, P. Wust, H. Fahling, J. Krause, W. Wlodarczyk, B. Sander, T. Vogl, R. Felix, *Int. J. Hyperthermia* **1997**, *13*, 587–605.
[151] L. R. Hirsch, R. J. Stafford, J. A. Bankson, S. R. Sershen, B. Rivera, R. E. Price, J. D. Hazle, N. J. Halas, J. L. West, *Proc. Natl. Acad. Sci. USA* **2003**, *100*, 13549–13554.
[152] X. H. Huang, I. H. El-Sayed, W. Qian, M. A. El-Sayed, *J. Am. Chem. Soc.* **2006**, *128*, 2115–2120.
[153] M. P. Melancon, W. Lu, Z. Yang, R. Zhang, Z. Cheng, A. M. Elliot, J. Stafford, T. Olson, J. Z. Zhang, C. Li, *Mol. Cancer Ther.* **2008**, *7*, 1730–1739.
[154] J. Nam, N. Won, H. Jin, H. Chung, S. Kim, *J. Am. Chem. Soc.* **2009**, *131*, 13639–13645.
[155] W. James, L. Hirsch, J. West, P. O'Neal, J. Payne, *J. Radioanal. Nucl. Chem.* **2007**, *271*, 455–459.
[156] R. Bernardi, A. Lowery, P. Thompson, S. Blaney, J. West, *J. Neuro-Oncology* **2008**, *86*, 165–172.
[157] A. R. Lowery, A. M. Gobin, E. S. Day, N. J. Halas, J. L. West, *Int. J. Nanomed.* **2006**, *1*, 149–154.
[158] J. Kim, S. Park, J. E. Lee, S. M. Jin, J. H. Lee, I. S. Lee, I. Yang, J. S. Kim, S. K. Kim, M. H. Cho, T. Hyeon, *Angew. Chem. Int. Ed.* **2006**, *45*, 7754–7758.
[159] R. Bardhan, W. X. Chen, C. Perez-Torres, M. Bartels, R. M. Huschka, L. L. Zhao, E. Morosan, R. G. Pautler, A. Joshi, N. J. Halas, *Adv. Funct. Mater.* **2009**, *19*, 3901–3909.
[160] M.-R. Choi, K. J. Stanton-Maxey, J. K. Stanley, C. S. Levin, R. Bardhan, D. Akin, S. Badve, J. Sturgis, J. P. Robinson, R. Bashir, N. J. Halas, S. E. Clare, *Nano Lett.* **2007**, *7*, 3759–3765.
[161] T. Kong, J. Zeng, X. P. Wang, X. Y. Yang, J. Yang, S. McQuarrie, A. McEwan, W. Roa, J. Chen, J. Z. Xing, *Small* **2008**, *4*, 1537–1543.
[162] H. Matsudaira, A. Ueno, I. Furuno, *Radiat. Res.* **1980**, *84*, 144–148.
[163] J. F. Hainfeld, D. N. Slatkin, H. M. Smilowitz, *Phys. Med. Biol.* **2004**, *49*, N309–N315.
[164] M. Y. Chang, A. L. Shiau, Y. H. Chen, C. J. Chang, H. H. W. Chen, C. L. Wu, *Cancer Sci.* **2008**, *99*, 1479–1484.
[165] X. J. Zhang, J. Z. Xing, J. Chen, L. Ko, J. Amanie, S. Gulavita, N. Pervez, D. Yee, R. Moore, W. Roa, *Clin. Invest. Med.* **2008**, *31*, E160–E167.
[166] S. H. Cho, *Phys. Med. Biol.* **2005**, *50*, N163–N173.
[167] S. H. Cho, B. L. Jones, S. Krishnan, *Phys. Med. Biol.* **2009**, *54*, 4889–4905.
[168] J. C. Roeske, L. Nunez, M. Hoggarth, E. Labay, R. R. Weichselbaum, *Technol. Cancer Res. Treat.* **2007**, *6*, 395–401.

[169] P. Mroz, G. P. Tegos, H. Gali, T. Wharton, T. Sarna, M. R. Hamblin, *Photochem. Photobiol. Sci.* **2007**, *6*, 1139–1149.
[170] H. Tokuyama, S. Yamago, E. Nakamura, T. Shiraki, Y. Sugiura, *J. Am. Chem. Soc.* **1993**, *115*, 7918–7919.
[171] P. Mroz, A. Pawlak, M. Satti, H. Lee, T. Wharton, H. Gali, T. Sarna, M. R. Hamblin, *Free Radical Biol. Med.* **2007**, *43*, 711–719.
[172] F. Rancan, S. Rosan, F. Boehm, A. Cantrell, M. Brellreich, H. Schoenberger, A. Hirsch, F. Moussa, *J. Photochem. Photobiol. B* **2002**, *67*, 157–162.
[173] Y. Tabata, Y. Murakami, Y. Ikada, *Cancer Sci.* **1997**, *88*, 1108–1116.
[174] J. Liu, S.-i. Ohta, A. Sonoda, M. Yamada, M. Yamamoto, N. Nitta, K. Murata, Y. Tabata, *J. Control. Release* **2007**, *117*, 104–110.
[175] A. C. S. Samia, X. Chen, C. Burda, *J. Am. Chem. Soc.* **2003**, *125*, 15736–15737.
[176] R. Bakalova, H. Ohba, Z. Zhelev, T. Nagase, R. Jose, M. Ishikawa, Y. Baba, *Nano Lett.* **2004**, *4*, 1567–1573.
[177] M. M. Stevens, *Nat. Nanotechnol.* **2009**, *4*, 342–343.
[178] K. Unfried, C. Albrecht, L. O. Klotz, A. Von Mikecz, S. Grether-Beck, R. P. F. Schins, *Nanotoxicol.* **2007**, *1*, 52–71.
[179] G. Oberdorster, V. Stone, K. Donaldson, *Nanotoxicol.* **2007**, *1*, 2–25.
[180] A. M. Derfus, W. C. W. Chan, S. N. Bhatia, *Nano Lett.* **2004**, *4*, 11–18.
[181] E. E. Connor, J. Mwamuka, A. Gole, C. J. Murphy, M. D. Wyatt, *Small* **2005**, *1*, 325–327.
[182] R. Hardman, *Environ. Health Perspect.* **2006**, *114*, 165–172.
[183] K.-T. Yong, H. Ding, I. Roy, W.-C. Law, E. J. Bergey, A. Maitra, P. N. Prasad, *ACS Nano* **2009**, *3*, 502–510.
[184] F. Erogbogbo, K. T. Yong, I. Roy, G. X. Xu, P. N. Prasad, M. T. Swihart, *Acs Nano* **2008**, *2*, 873–878.
[185] A. Burns, H. Ow, U. Wiesner, *Chem. Soc. Rev.* **2007**, *35*, 1028–1042.
[186] H. Ow, D. R. Larson, M. Srivastava, B. A. Baird, W. W. Webb, U. Wiesner, *Nano Lett.* **2004**, *5*, 113–117.
[187] X. L. Chen, M. C. Estevez, Z. Zhu, Y. F. Huang, Y. Chen, L. Wang, W. H. Tan, *Anal. Chem.* **2009**, *81*, 7009–7014.
[188] J. Liu, A. Stace-Naughton, X. Jiang, C. J. Brinker, *J. Am. Chem. Soc.* **2009**, *131*, 1354–1355.
[189] European Nanotechnology Gateway, www.nanoforum.org (last accessed on August 18, 2010).
[190] Scientific Opinion of the Scientific Committee on a request from the European Commission on the Potential Risks Arising from Nanoscience and Nanotechnologies on Food and Feed Safety, *The EFSA Journal* **2009**, *958*, 1-39.
[191] J. Cardinal, J. R. Klune, E. Chory, G. Jeyabalan, J. S. Kanzius, M. Nalesnik, D. A. Geller, *Surgery* **2008**, *144*, 125–132.
[192] I. Hilger, R. Hiergeist, R. Hergt, K. Winnefeld, H. Schubert, W. A. Kaiser, *Investigative Radiology* **2002**, *37*, 580–586.
[193] J. Manfred, T. Burghard, J. Andreas, T. Kasra, G. Uwe, W. Norbert, S. Regina, K. Martin, L. Michael, J. Klaus, A. L. Stefan, *The Prostate* **2005**, *64*, 283–292.
[194] T. Ohno, T. Wakabayashi, A. Takemura, J. Yoshida, A. Ito, M. Shinkai, H. Honda, T. Kobayashi, *J. Neuro-Oncology* **2002**, *56*, 233–239.
[195] M. Yanase, M. Shinkai, H. Honda, T. Wakabayashi, J. Yoshida, T. Kobayashi, *Jpn. J. Cancer Res.* **1998**, *89*, 775–782.
[196] P. P. Macaroff, D. M. Oliveira, Z. G. M. Lacava, E. C. D. Lima, P. C. Morais, A. C. Tedesco, *J. Appl. Phys.* **2005**, *97*, 10Q906.

Received: March 30, 2010
Published online: September 27, 2010

